



A Very Large-Eddy Simulation (VLES) model for the investigation of the neutral atmospheric boundary layer

Amir A. Aliabadi^{a,*}, Nikolaos Veriotes^a, Gonalo Pedro^b

^a Environmental Engineering, University of Guelph, Guelph, Canada

^b RWDI Consulting Engineers and Scientists, Guelph, Canada

ARTICLE INFO

Keywords:

atmospheric boundary layer (ABL)
Computational fluid dynamics (CFD)
Turbulence
Very large-eddy simulation (VLES)

ABSTRACT

A Very Large Eddy Simulation (VLES) model is developed for the investigation of the Atmospheric Boundary Layer (ABL) under thermally neutral conditions. The development approach is reductionist aimed at minimizing the number of input parameters for the model while attempting to simulate mean flow, turbulence statistics, spectra, and anisotropy realistically. The VLES model has been tested against experimental wind tunnel data and other LES models. It has been verified that the model can reproduce experimental profiles of mean velocity and turbulence velocity statistics reasonably well. It also simulates spectra and anisotropy realistically. The VLES model shows potential for use in industrial applications where it is impractical to perform high resolution simulations or implement complex synthetic inlet conditions to match all flow properties beyond what is necessary for a particular application. This model is ideal for transport applications (e.g. air pollution dispersion) while further investigation is required if it is to be used for wind-induced structural loading.

1. Introduction

Large Eddy Simulation (LES) has been demonstrated to be very effective in accurately simulating turbulent flows for applications where eddy viscosity models or direct numerical simulations are either too inaccurate or too computationally expensive, respectively (Aliabadi, 2018). Atmospheric Boundary Layer (ABL) flows at micro or limited regional scales are a class of flows that have been investigated using LES since a few decades ago (Smagorinsky, 1963). Although higher computational power has been made available for LES models of flows of greater scales and turbulence levels during the last few decades, still a standard LES is seldom possible for most practical flows. For instance, most practical flow simulations are not driven by perfectly realistic perturbation fields in their inlet boundary conditions, do not resolve turbulent fluctuations down to the finest scales of the inertial subrange, and are not wall-resolving. Such limitations are usually circumvented by the use of

case-specific inlet boundary conditions, Sub-Grid Scale (SGS) models, and wall treatments. In the following subsections, a brief literature review of methods addressing each of the above model components is provided.

1.1. Inlet boundary conditions

The LES model requires turbulent fluctuations at the inlet that would evolve in the model domain for realistic simulation of the turbulent flow. From a theoretical stand point, the fluctuations must meet several criteria: a) they must be stochastically varying, on scales down to the spatial and temporal filter scales; b) they must be compatible with the Navier-Stokes equations; c) they must be composed of coherent eddies across a range of spatial scales down to the filter length; d) they must allow easy specification of turbulence properties; and e) they must be easy to implement (Tabor and Baba-Ahmadi, 2010). Two common

Abbreviations: Atmospheric Boundary Layer, ABL; Consistent Discrete Random Field Generation, CDRFG; Computational Fluid Dynamics, CFD; Large-Eddy Simulation, LES; Modified Discretizing and Synthesizing Random Flow Generation, MDSRFG; Open source Field Operation And Manipulation, OpenFOAM; Sub-Grid Scale, SGS; Turbulence Kinetic Energy, TKE; Very Large Eddy Simulation, VLES; Wall-Adapted Local Eddy, WALE; Weather Research and Forecasting, WRF.

* Corresponding author.

E-mail address: aliabadi@uoguelph.ca (A.A. Aliabadi).

URL: <https://www.aaa-scientists.com> (A.A. Aliabadi).

<https://doi.org/10.1016/j.jweia.2018.10.014>

Received 29 May 2018; Received in revised form 30 August 2018; Accepted 18 October 2018

approaches that generate inlet turbulent fluctuations for LES models are the synthetic and precursor methods. In the synthetic method, random fields are constructed at the inlet, while in the precursor method a simulation is performed to generate the desired fluctuations.¹ Precursor methods are shown to be more accurate but more computationally demanding and more difficult to implement (Tabor and Baba-Ahmadi, 2010). While precursor methods have been reviewed elsewhere in the literature (Thomas and Williams, 1999; Tabor and Baba-Ahmadi, 2010; Castro and Paz, 2013), this section only reviews a selected number of synthetic methods in the literature chronologically.

The method of Lund et al. (1998), which was originally developed by Spalart (1988), generates inflow turbulence by rescaling the velocity field at a downstream station, and re-introducing it as a boundary condition at the inlet, and hence developing spatial and temporal turbulent boundary layers economically (Lund et al., 1998; Cao, 2014). This method has also been extended for rough-wall conditions by Nozawa and Tamura (2002), and for inclusion of gravity waves in ABL simulations by Mayor et al. (2002). Compared to primitive methods, e.g. random inclusion of perturbations at inlet, it has been shown that the method reduces adaptation distance upstream of the flow down to ten times the boundary-layer height (Lund et al., 1998; Mayor et al., 2002).

The vortex method originally developed by Sergent (2002) and later refined by Benhamadouche et al. (2006), Mathey et al. (2006), and Xie (2016) inserts random two-dimensional vortices at the inlet boundary that evolve into the simulation domain. These vortices are parameterized by realistic lengthscales, timescales, and vorticity magnitudes, formulated from mean flow information and grid spacing. This method has been shown to work well in channel, pipe, and back step flows, where the primary concern is the evolution and magnitude of the turbulence variances and fluxes as a function of wall-normal distance in the flow.

The method of Kim et al. (2013) extends inflow conditions formulated on a two-dimensional plane at the inlet to modifications on an adjacent plane near the inlet as well to reduce unphysical large pressure fluctuations in the domain, as would otherwise be expected from an inflow condition formulated purely on a two-dimensional plane. This divergence-free method is shown to provide reasonable time-averaged turbulence variances and fluxes, suitable for many applications.

Another divergence-free method originally developed by Jarrin (2008) and further refined by Poletto et al. (2013) aims to reproduce any state of Reynolds stress anisotropy as a function of the characteristic ellipsoid eddy shapes described by an aspect ratio. Results from turbulent channel flow indicate reduced pressure fluctuations in the streamwise direction and reduced flow adaption distance down to less than ten boundary-layer heights.

For ABL simulations, another approach is to nest an LES model within a larger domain mesoscale model such as the Weather Research and Forecasting (WRF) model (Mirocha et al., 2014). In such models, the inlet condition is either provided by the mesoscale model without perturbations, or alternatively a random fluctuation field is superimposed on the inlet condition. In addition, perturbations can be added by specifying non-homogeneous surface fluxes of momentum or heat. It has been shown that perturbations are still necessary to generate and maintain turbulence in the LES domain, regardless of nesting. In addition, the best perturbation method will depend on the type of SGS parameterization (Mirocha et al., 2014).

The method of Aboshosha et al. (2015b) is based on synthesizing random divergence-free turbulence velocities with consideration of spectra and coherency functions that match the ABL flow statistics. The method is also known as Consistent Discrete Random Field Generation

(CDRFG). This scheme maintains both the turbulence spectra and coherency function, which are essential for proper simulation of interaction of turbulent ABL flow with flexible structures, such as buildings, prone to wind-induced dynamic excitation.

Most recently, newer synthetic methods known as Modified Discretizing and Synthesizing Random Flow Generation (MDSRFG) attempt a correct representation of the coherence of the velocity field (Castro et al., 2017; Ricci et al., 2017). These methods are particularly useful for analysis of wind-induced excitation of tall buildings. The method, as applied for turbulent flow simulations around rectangular blocks, yields a realistic representation of spatially correlated velocities in the domain (Castro et al., 2017). The method also describes the effect of wind angle of attack and the subsequent dynamic structural response (Ricci et al., 2017).

As an alternative to velocity perturbation, the temperature perturbation method, developed by Buckingham et al. (2017), can be used to develop turbulent flow structures near the inlet by buoyancy driven mechanisms. It has been shown that this alternative can result in adaptation distances up to fifteen boundary-layer heights, not requiring prior knowledge of second order moments or integral lengthscales at the inlet.

1.2. Sub-grid scale (SGS) model

The oldest yet very common SGS model is the Smagorinsky (1963) model where the momentum transport by the unresolved velocity field is parameterized by an effective viscosity (Aliabadi, 2018). Various SGS models employ the Smagorinsky (1963) model (Lund et al., 1998; Fröhlich et al., 2005; Benhamadouche et al., 2006; Aboshosha et al., 2015b). Other SGS models include the Wall-Adapted Local Eddy-viscosity (WALE) model used by various investigators (Fröhlich et al., 2005), and the one-equation SGS Turbulence Kinetic Energy (TKE) model that has gained popularity recently (Li et al., 2008, 2010; 2012, 2015; Aliabadi et al., 2017).

1.3. Wall functions

The hypothesis of wall similarity for smooth-wall and rough-wall boundary layers in the outer layer have been successfully confirmed for flows that meet several criteria: 1) the flow exhibits a high Reynolds number (Raupach et al., 1991), lower limit of which depends on the specific way the Reynolds number is defined, 2) the blockage ratio, defined as the depth of the boundary layer δ over the characteristic roughness length h satisfies $\delta/h > 40 - 80$ (Jiménez, 2004), and 3) the roughness structure is geometrically simple and horizontally homogeneous over smoothly varying topography (Anderson and Meneveau, 2010; Aboshosha et al., 2015a). This has enabled wall functions to be used for a long time to economize Computational Fluid Dynamics (CFD) simulations (Launder and Spalding, 1974). There are two main types of roughness modifications for rough walls where wall similarity laws hold (Blocken et al., 2007). The first is the law of the wall based on sand grain roughness scale k_s with widespread application within the engineering community (Jiménez, 2004; Blocken et al., 2007; Krogstad and Efron, 2012). Alternatively, meteorologists have used a wall function utilizing the aerodynamics roughness length scale z_0 (Raupach et al., 1991; Kent et al., 2017). Often a displacement height d is used to correct the height with $z - d$ (Raupach et al., 1991; Amir and Castro, 2011; Graf et al., 2014), in which case the surface normal non-dimensional distance is $(z - d)^+ = (z - d)u_\tau/\nu$, where u_τ is friction velocity and ν is kinematic viscosity. For moderate roughness density it has been shown that the aerodynamic roughness length and displacement height form the following relationships with the actual roughness element characteristic height h : $z_0/h \approx 0.1$ and $d/h \approx 0.8$ (Raupach et al., 1991). Many variates of wall functions discussed above predict a log-law, i.e. a linear relationship between $U^+ = U/u_\tau$ and logarithm of z^+ . Various upper limits have been reported for the z^+ to satisfy the log-law. Conservative

¹ Note that applying periodic boundary conditions in the streamwise direction may be interpreted as a form of precursor method. In such methods the fluctuations reentering the domain are often filtered or further statistically manipulated. For instance to prevent wakes, generated in the domain, from entering the domain filtering techniques are often used (Thomas and Williams, 1999).

estimates suggest $z^+ < 500 - 1000$ applicable to smooth and very rough walls with intercept adjustments (Blocken et al., 2007). For instance the LES model of Thomas and Williams (1999) uses $z^+ \approx 800$. Non-conservative upper limits have been shown to exhibit a near log-law behaviour for $z^+ \rightarrow 10000$ (Kays and Crawford, 1993).

If wall similarity cannot be established, and hence a simple parameterization of a wall function is not possible, then numerous approaches can be used to model transport phenomena near the walls. For example, a roughness structure can be explicitly resolved (Jiménez, 2004; Aboshosha et al., 2015a); canopy models may be developed (Aboshosha et al., 2015a); terrain-following coordinate systems may be utilized (Anderson and Meneveau, 2010); different wall functions can be aggregated in neighbouring patches of the surface with different roughness structures (Anderson and Meneveau, 2010); and a drag force can be parameterized given roughness structure shape, plan and frontal area densities, or other properties that vary horizontally (Raupach, 1992; Martilli et al., 2002; Anderson and Meneveau, 2010; Krayenhoff et al., 2015).

1.4. Objective

The objective of this study is to develop a Very Large Eddy Simulation (VLES) model for the investigation of the atmospheric boundary layer and to validate its performance against wind tunnel measurements and other LES models by matching mean and turbulence profiles related to the momentum. The objectives require that the model 1) should be practical with a reductionist approach requiring minimum number of input constants, namely the reference height and velocity, only two constants specifying the inlet fluctuation length and time scales, and aerodynamic roughness length scale, 2) should simulate anisotropic boundary layer turbulence by demonstrating that the turbulence statistics are direction dependent, 3) should resolve the energy cascade over at least two orders of magnitude of wave numbers, namely simulating transfer of energy from energy-containing subrange down to the inertial subrange, 4) should demonstrate that the correlation for velocity fluctuation components are wave-number dependent with higher correlation for lower wave numbers, 5) should avoid resolving turbulence near walls by use of wall functions to prevent excessive computational cost, and 6) should exhibit a low adaptation distance, requiring an upstream distance shorter than five boundary-layer heights to establish a turbulent boundary layer for practical applications.

The VLES model development has three main components: 1) in Sect. 2.2 we discuss the implementation of a synthetic vortex method as an inlet boundary condition, 2) in Sect. 2.3 we discuss the implementation of an SGS model, and 3) in Sect. 2.4 we discuss the choice of a wall function. The specifics of the numerical schemes and methodologies are discussed in Sect. 2.5. Sect. 3.1 presents the results of smooth surface wall-resolving simulations. In Sect. 3.1.1 we discuss the results for a series of computational runs of the model with various levels of grid coarsening. In Sect. 3.1.2 and 3.1.3 the effect of parameters defining the synthetic vortex method and SGS model are studied in various sensitivity tests. In Sect. 3.1.4 and 3.1.5 the spectral content and isotropy of turbulence are discussed for the smooth surface wall-resolving simulations. Sect. 3.2 presents the results of rough-wall simulations with wall functions. The sensitivity of the model to coarsening of the first layer of computational grid is studied in Sect. 3.2.1. In Sect. 3.2.2 and 3.2.3 the spectral content and isotropy of turbulence are discussed for the rough-wall simulations with wall function. In Sect. 3.2.4 the sensitivity of the model to changing the aerodynamic roughness length is studied. Conclusions and future work are stated in Sect. 4.

Such investigations are seldom performed for VLES models applicable to ABL studies systematically (Blocken et al., 2011), which is a focus of this study and can inform future VLES model development efforts. The simulations are developed using the CFD software Open source Field Operation And Manipulation (OpenFOAM) version 4.0.

2. Methodology

2.1. Model geometry

The model geometry is shown in Fig. 1. The tunnel height, width, and length are $Z = 1$ m, $Y = 1$ m, and $X = 5$ m, respectively. Airflow is in the x direction. Four vertical solution probes are envisioned for monitoring the simulation results. The boundary conditions, initial conditions, and discretization details are described in Sect. 2.5.

2.2. The synthetic vortex method

To generate turbulence at the inlet a vortex method is used. The original version used here is developed by Sergent (2002) and has been continually improved until recently (Xie, 2016). The main idea of the vortex method is to generate velocity fluctuations in the form of synthetic eddies derived from mean statistical information about the flow as a function of space (height above ground) and time. To economize the approach a vortex field is inserted at the inlet that does not require a precursor simulation or implementation of a cyclic boundary condition at inlet-outlet faces. The controlling parameters are the number of vortices, the size of each vortex, the vorticity (or equivalently velocity field characterizing each vortex), and the lifetime of vortices (Mathey et al., 2006).

The vortex method uses vortices on the inlet boundary to generate velocity fluctuations. The vortices are two dimensional with their vorticity vector parallel to the streamwise direction. The theory is fully developed in the literature (Sergent, 2002; Mathey et al., 2006; Benhamadouche et al., 2006; Xie, 2016) and provides the following velocity fluctuation field for a given timestep

$$\mathbf{u}(\mathbf{x}) = \frac{1}{2\pi} \sum_{i=1}^N \Gamma_i \frac{(\mathbf{x}_i - \mathbf{x}) \times \mathbf{s}}{|\mathbf{x}_i - \mathbf{x}|^2} \left(1 - e^{-\frac{|\mathbf{x}_i - \mathbf{x}|^2}{2(\sigma_i(\mathbf{x}_i))^2}} \right) e^{-\frac{|\mathbf{x}_i - \mathbf{x}|^2}{2(\sigma_i(\mathbf{x}_i))^2}}, \quad (1)$$

where \mathbf{u} is velocity perturbation at the model inlet that is later superimposed on the mean inlet velocity, \mathbf{x} is position vector on the inlet boundary, N is the number of vortices to be inserted at the inlet (we use $N = 200$ exclusively), i is the index for the current vortex, Γ_i is the circulation for the current vortex, \mathbf{x}_i is the position vector for the centre of the current vortex, \mathbf{s} is unit vector along the streamwise direction, and $\sigma_i(\mathbf{x}_i)$ is a characteristic length for the radius of current vortex. This formula essentially superimposes velocity fluctuation fields from N vortices to provide an overall perturbation velocity field at the inlet. The specific parameterizations required to develop models for each term in this formula will be provided below.

We assume that the wall-normal direction is $+z$ and that flow is in the $+x$ direction. A power-law profile is assumed for the mean velocity (Thomas and Williams, 1999; Ricci et al., 2017) given by

$$\overline{U}(z) = U_{ref} \left(\frac{z}{z_{ref}} \right)^\alpha, \quad (2)$$

where z_{ref} is a reference height, U_{ref} is reference velocity, and α is an exponent parameterized as a function of aerodynamic roughness length. In fact there is a functional relationship between exponent α and the characteristic aerodynamic roughness length of the surface z_0 (Thomas and Williams, 1999; Aliabadi, 2018) given as

$$\alpha = \frac{1}{\ln\left(\frac{z_{ref}}{z_0}\right)}. \quad (3)$$

Next a turbulence intensity profile has to be assumed. This is obtained from the relationship

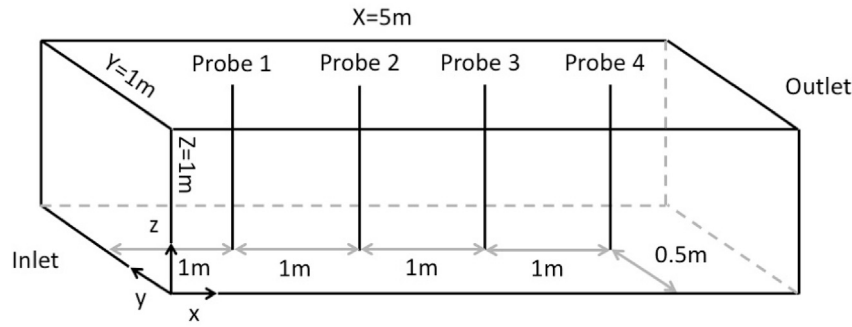


Fig. 1. VLES case geometry and solution monitoring probes.

$$I_u(z) = \frac{1}{\ln\left(\frac{z}{z_0}\right)}, \quad (4)$$

where $I_u(z)$ is limited by a maximum value $I_{u,max}$ given the fact that for atmospheric flows there is a limit to $I_u(z)$ of typically in the order of one (Stull, 1998; Nozawa and Tamura, 2002; Aliabadi et al., 2018). Particularly, with decreasing z_0 , the formulation above gives rise to very unrealistically large $I_u(z)$ values near the surface as $z \rightarrow 0$. This must be avoided by setting the $I_{u,max}$ limit. This allows parameterization of sub-grid TKE (k) such that

$$k(z) = 1.5(U(z)I_u(z))^2. \quad (5)$$

To calculate characteristic size for the energy-containing eddies or vortices, we first approximate a characteristic length for the inlet boundary

$$L = \frac{2L_z L_y}{L_z + L_y}, \quad (6)$$

where L_z and L_y are inlet height and width. It is reasonable to assume that the size of the largest energy-containing vortices, i.e. σ_{max} , scales with L because for atmospheric boundary layer flow simulations the boundary layer height δ is in the order of L for economized models. We relate σ_{max} and L using a constant a_σ , to be adjusted later, with

$$\sigma_{max} = a_\sigma L. \quad (7)$$

For VLES, it must be ensured that grid spacing Δ in the coarsest region of mesh, likely on top of the domain, satisfies $\Delta < \sigma_{max}$ (Xie, 2016) since the VLES model should be able to resolve the transport, dynamics, and breakdown of the largest eddies in the flow. On the other hand, the size of energy-containing vortices or eddies is a function of height and must

Table 1
Numerical grids for CFD cases.

Grid Level	$N_x-N_y-N_z$	N_{Total}
I	100 – 100 – 100	1,000,000
II	100 – 75 – 75	562,500
III	100 – 50 – 50	250,000
IV	100 – 25 – 25	62,500

Table 2
Boundary-layer bulk features for the smooth surface wall-resolving simulations. For each grid level, a range of results are provided for profiles 1, 2, 3, and 4.

Grid Level	I	II	III	IV
u_τ [m s ⁻¹]	0.057-0.081	0.065-0.086	0.065-0.086	0.060-0.083
δ [m]	0.941	0.922	0.941	0.791
δ^* [m]	0.150-0.152	0.149-0.153	0.149-0.152	0.127-0.136
θ [m]	0.106-0.108	0.107-0.108	0.105-0.108	0.093-0.100
Re_θ	10,200–10,500	10,100–10,400	10,100–10,400	8900–9500
Δ [m]	2.89-4.15	2.67-3.59	2.67-3.59	2.42-3.40

decrease with decreasing height. Energy-containing vortex size is parameterized using the mixing length approach of Mellor and Yamada (1974) such that

$$\frac{1}{\sigma(z)} = \frac{1}{\sigma_{max}} + \frac{1}{\kappa(z + z_0)}, \quad (8)$$

where, $\kappa = 0.41$ is the von Kármán constant. This formulation implies that $\sigma(z) \rightarrow \kappa z_0$ as $z \rightarrow 0$ and $\sigma(z) \rightarrow \sigma_{max}$ as $z \rightarrow \infty$. It is apparent that $\sigma(z) = \sigma(x)$ is designed to represent the energy-containing eddy size at each height above ground for the synthetic vortex method, and it is incumbent upon the simulation to create the energy cascade, down to the local grid size Δ , within a short adaptation distance downstream of the inlet.

A characteristic time for the largest energy-containing vortices or eddies can be approximated using scaling. The characteristic velocity U_0 for the largest energy-containing eddies can be defined using the power-law and the reference height $U_0 = a z_{ref}^\alpha$. The lengthscale for such eddies can also be found using our definition $\ell_0 = \sigma_{max}$. These two scales allow calculation of the Reynolds number for the largest energy-containing eddies $Re_{\ell_0} = U_0 \ell_0 / \nu$. These provide estimates for the Kolmogorov lengthscale $\eta = \ell_0 Re_{\ell_0}^{-3/4}$, Kolmogorov velocity scale $u_\eta = U_0 Re_{\ell_0}^{-1/4}$, and dissipation rate $\varepsilon = \nu(u_\eta/\eta)^2$. This provides the characteristic lifetime for the largest energy-containing eddies in the flow as

$$\tau_0(\ell_0) = \left(\frac{\ell_0^2}{\varepsilon}\right)^{1/3}. \quad (9)$$

This timescale is not representative for all energy-containing vortices or eddies, but only the largest ones. For ease of implementation, it is possible to define a representative time scale for all energy-containing eddies assuming a constant a_τ , to be adjusted later, with

$$\tau = a_\tau \tau_0(\ell_0). \quad (10)$$

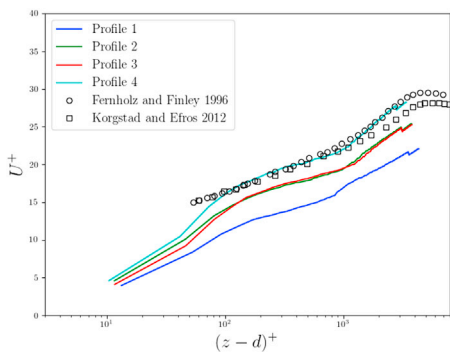
This timescale can be used to sample a new set of vortices at the inlet after every fixed number of iterations, when this timescale is elapsed.

The circulation can also be parameterized for each vortex knowing the face area S of the numerical cell at which a vortex is centred and TKE (k) given for a height. The circulation sign is randomized as either positive or negative for each vortex.

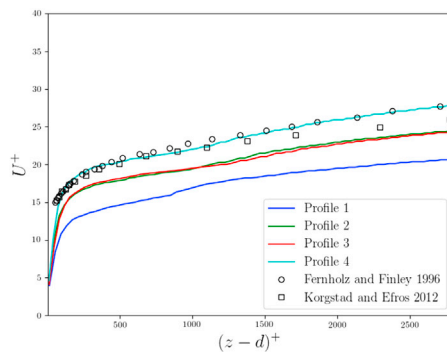
$$\Gamma = 4 \left(\frac{\pi S k}{3N(2 \ln 3 - 3 \ln 2)} \right)^{1/2}. \quad (11)$$

2.3. Implementation of sub-grid scale (SGS) model

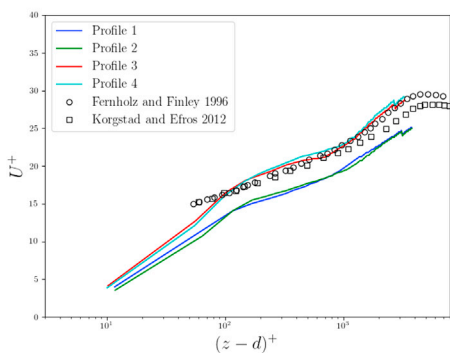
An incompressible turbulent flow based on a one-equation SGS model is considered. The dimensionless Navier-Stokes equations are developed and discussed below using a reference length scale such as the boundary-layer height δ and the reference upstream velocity U_0 . With this model, the continuity equation becomes



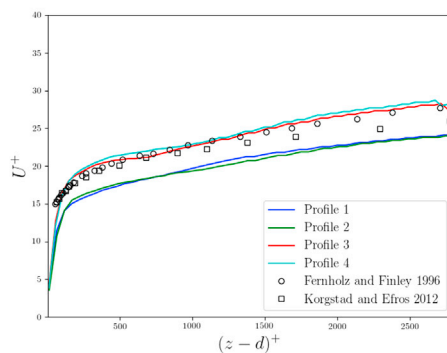
(a) $N = 1,000,000$ (Level I)



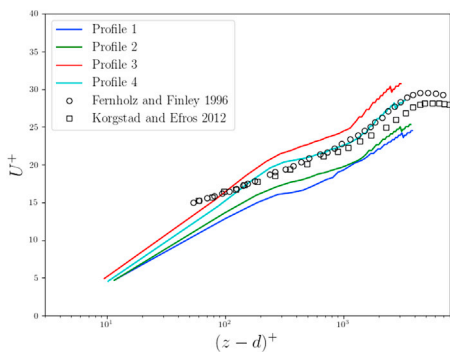
(b) $N = 1,000,000$ (Level I)



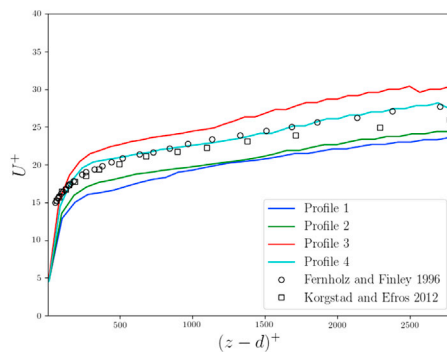
(c) $N = 562,500$ (Level II)



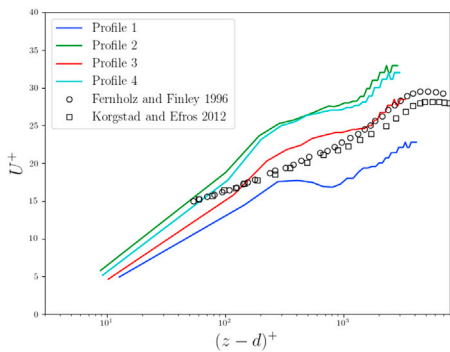
(d) $N = 562,500$ (Level II)



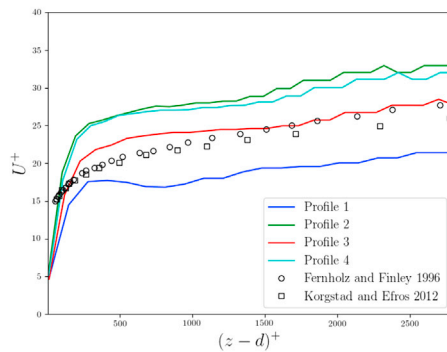
(e) $N = 250,000$ (Level III)



(f) $N = 250,000$ (Level III)

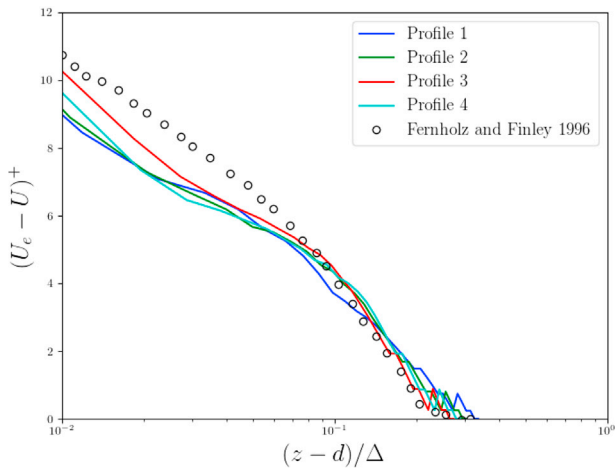


(g) $N = 62,500$ (Level IV)

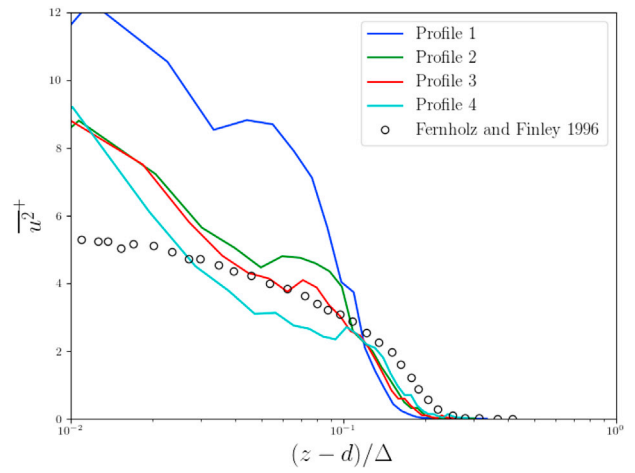


(h) $N = 62,500$ (Level IV)

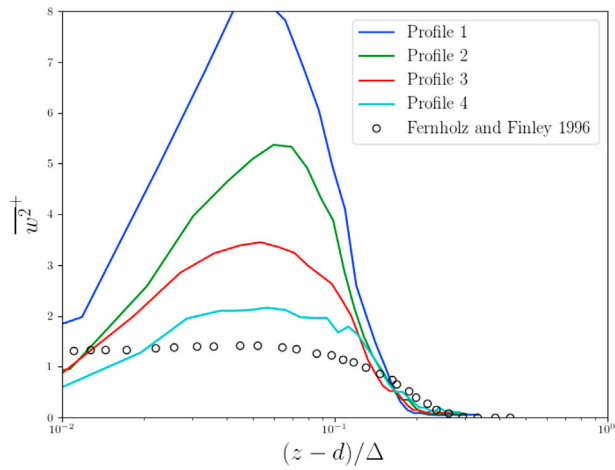
Fig. 2. Non-dimensionalized horizontal mean velocity vs. non-dimensionalized wall-normal distance for different grid levels in both logarithmic (a, c, e, g) and linear (b, d, f, h) scales.



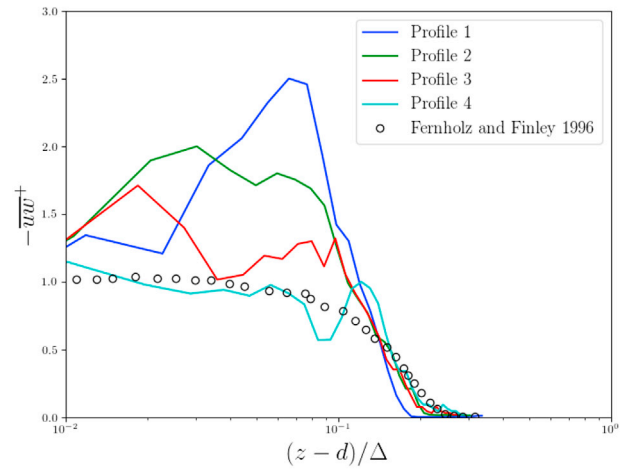
(a) Mean Horizontal Velocity Defect



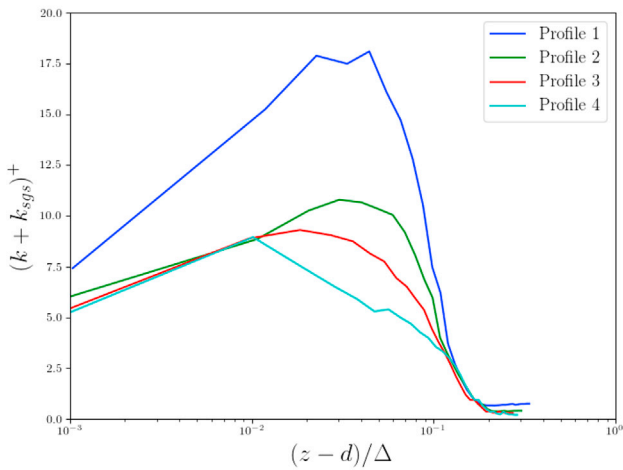
(b) Horizontal Velocity Variance



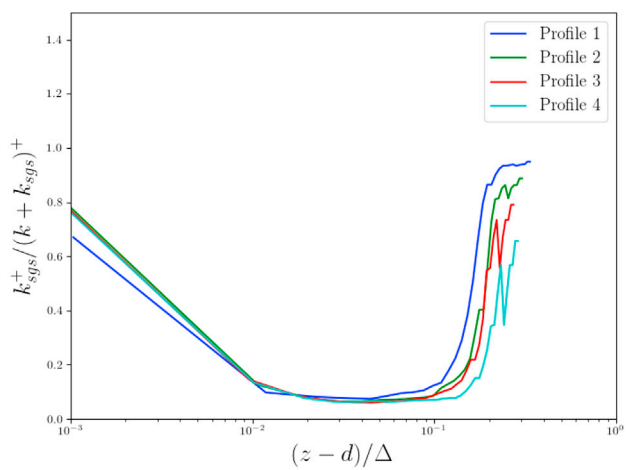
(c) Vertical Velocity Variance



(d) Reynolds Stress



(e) Total TKE



(f) TKE Ratio

Fig. 3. Non-dimensionalized turbulence statistics vs. non-dimensionalized wall-normal distance using the Clauser scaling parameter for wall-resolving simulations at grid level III.

$$\frac{\partial \bar{U}_i}{\partial x_i} = 0, \quad (12)$$

where the overbar notation signifies the spatially- and temporally-resolved velocity. The momentum and SGS TKE equations become

$$\frac{\partial \bar{U}_i}{\partial t} + \frac{\partial}{\partial x_j} \bar{U}_i \bar{U}_j = -\frac{\partial \bar{p}}{\partial x_i} - \frac{\partial \tau_{ij}}{\partial x_j} + \frac{1}{Re} \frac{\partial^2 \bar{U}_i}{\partial x_j \partial x_j}, \quad (13)$$

$$\frac{\partial k_{sgs}}{\partial t} + \bar{U}_i \frac{\partial k_{sgs}}{\partial x_i} = P - \varepsilon + \frac{\partial}{\partial x_i} \left(\frac{2}{Re_T} \frac{\partial k_{sgs}}{\partial x_i} \right), \quad (14)$$

where \bar{U} is the spatially- and temporally-resolved velocity, k_{sgs} is SGS TKE, $Re = U_0 \delta / \nu$ is the Reynolds number, and $Re_T = U_0 \delta / \nu_T$ is the turbulence Reynolds number (Li et al., 2010). The symbol \bar{p} denotes the resolved-scale modified kinematic pressure, normalized by constant density

$$\bar{p} = \bar{p}^* + \frac{1}{3} \tau_{ii}, \quad (15)$$

where \bar{p}^* is the resolved-scale static pressure. Other quantities in the above equations are as follows

$$\tau_{ij} = \bar{U}_i \bar{U}_j - \bar{U}_i \bar{U}_j, \quad (16)$$

$$P = -\tau_{ij} \bar{S}_{ij}, \quad (17)$$

$$\varepsilon = C_\varepsilon \frac{k_{sgs}^{3/2}}{l}, \quad (18)$$

where τ_{ij} is the SGS momentum flux, P is the shear production, and ε is the dissipation rate. The new terms in these equations require further parametrization using

$$\bar{S}_{ij} = \frac{1}{2} \left(\frac{\partial \bar{U}_i}{\partial x_j} + \frac{\partial \bar{U}_j}{\partial x_i} \right), \quad (19)$$

$$\nu_T = C_k k_{sgs}^{1/2} l. \quad (20)$$

The turbulence model is closed by using parametrizations for the remaining quantities. C_k is taken to be 0.094, and C_ε is taken to be 1.048. The length scale is estimated as a function of local grid size but damped near the walls using van Driest damping functions to prevent excessive dissipation of TKE near the walls (van Driest, 1956). The lengthscale, not near the walls where damping functions are used, is formulated as

$$l = C_\Delta (\Delta x \Delta y \Delta z)^{1/3}, \quad (21)$$

where C_Δ is a parameter to control l and therefore the SGS model. The SGS momentum flux is parametrized using the eddy-viscosity assumption,

$$\tau_{ij} = -2\nu_T \bar{S}_{ij}. \quad (22)$$

This SGS model is known as oneEqnEddy in OpenFOAM.

2.4. The choice of wall function

The wall function chosen for the model is based on the environmental flow wall function given by (Raupach et al., 1991)

$$U^+ = \frac{1}{\kappa} \ln \left(\frac{z + z_0}{z_0} \right) \approx \frac{1}{\kappa} \ln \left(\frac{z}{z_0} \right), \quad (23)$$

where z_0 is characteristic aerodynamic roughness length of the surface, κ is the von Kármán constant, and U^+ is non-dimensional velocity in the streamwise direction. This wall function is known as

nutkAtmRoughWallFunction in OpenFOAM.

2.5. Numerical schemes

2.5.1. Numerical grid

Four numerical grids are considered for the simulations (see Table 1). These range from very fine with 1,000,000 control volumes to very coarse with 62,500 control volumes. The grid spacings in the x and y directions are uniform, while in the z direction, spacing is varied. The grid is generated using the blockMesh utility provided in OpenFOAM. A simple grading scheme in blockMesh calculates the cell sizes using a simple geometric progression so that along a length l , if n cells are requested with a ratio of $M > 1$ between the last and first cells, then the size of the smallest cell is $\delta x_s = l(r-1)/(Mr-1)$, where $r = M^{\frac{1}{n-1}}$ (Greenshields, 2015). A grading ratio of $M = 20$ is used in the z direction. The wall-adjacent grid height is tightly controlled and separately varied, independent of grading in the interior of the domain, so that the effect of using SGS model and wall functions can be studied independently by increasing or decreasing the height of the first grid layer independently. The grid spacing in the streamwise direction, i.e. x , is not changed in order to keep the aspect ratio of the cells low, as is recommended for LES studies of the ABL (Mirocha et al., 2014). This is particularly needed since the first layer of the grid is controlled separately, and generation of high aspect ratios are not desired when first layer height is kept constant while the grid is coarsened in all directions. Values for $(z-d)^+$ in the first layer are reported in Sect. 3.2.1 where wall functions are used, otherwise for wall-resolving simulations $(z-d)^+ < 5$.

2.5.2. Boundary conditions

For all solution variables, the zero-gradient condition is used for the top boundary and the cyclic condition is used for the front and back sides of the domain. For velocity, the synthetic vortex method, introduced in Sect. 2.2, is used at inlet, the no-slip condition is used at the domain bottom, and zero-gradient condition is used at the outlet.

For SGS TKE, the atmBoundaryLayerInletK boundary condition is used at inlet. This condition assumes that the entire inlet boundary is in the inertial surface layer of ABL such that the friction velocity and TKE are independent of height (Stull, 1988). This boundary condition first calculates the friction velocity, assuming the log-law, as

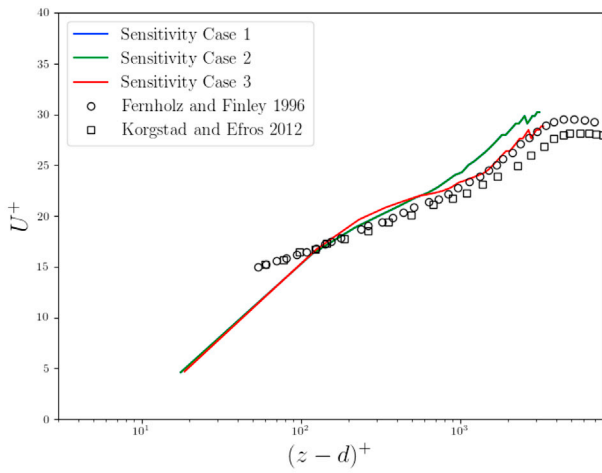
$$u_\tau = \frac{\kappa U_{ref}}{\ln \left(\frac{z_{ref} + z_0}{z_0} \right)}, \quad (24)$$

and then computes a uniform SGS TKE as $k_{sgs} = u_\tau^2 / C_\mu^{1/2}$, where $C_\mu = 0.09$ is a constant. Of course, much of the TKE is contained in the scales resolved by VLES, so it is expected that k_{sgs} will sharply drop in the streamwise direction near the inlet, but it will stabilize in the interior of the domain in the streamwise direction. Specification of k_{sgs} in this manner will provide a convenient method to develop the inlet condition for the synthetic vortex method. At the wall two conditions are possible, either zero value for wall-resolving simulations or the kqRWallFunction boundary condition for the use of standard wall functions. At the outlet the zero-gradient condition is used.

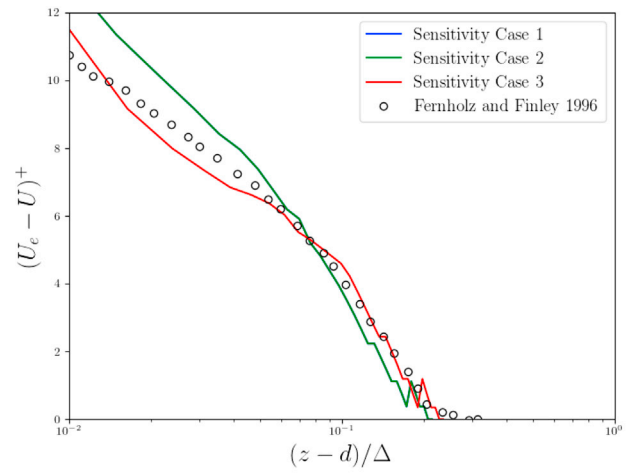
Table 3

Sensitivity of boundary-layer bulk features to a_σ for the smooth surface wall-resolving simulations. Grid level III is used and the results are provided for profile 4.

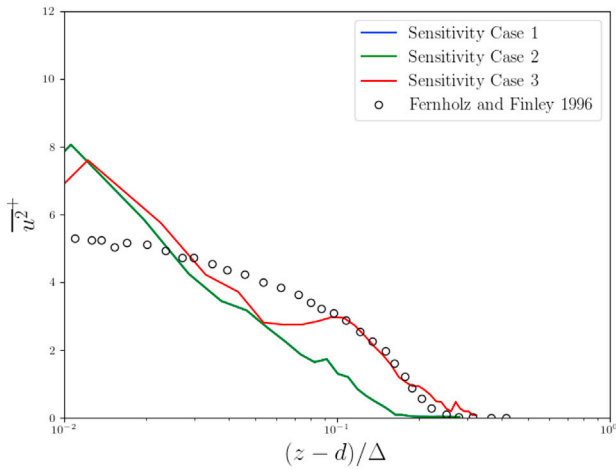
Constant	$a_\sigma = 0.1$	$a_\sigma = 0.2$	$a_\sigma = 0.3$
u_τ [m s ⁻¹]	0.068	0.068	0.068
δ [m]	0.941	0.941	0.941
δ^* [m]	0.152	0.152	0.146
θ [m]	0.107	0.107	0.105
Re_θ	10,400	10,400	10,200
Δ [m]	3.44	3.44	2.88



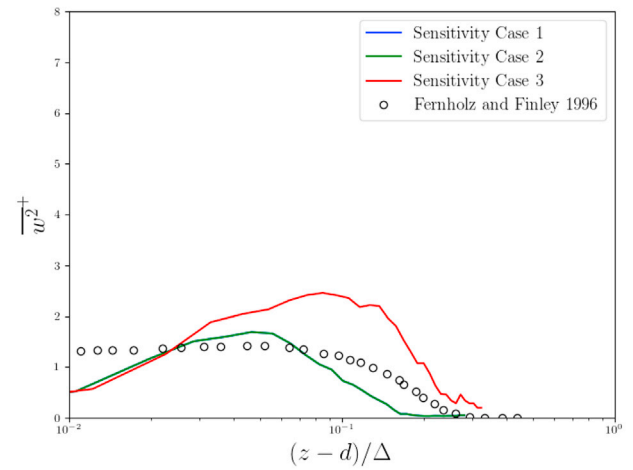
(a) Mean Horizontal Velocity



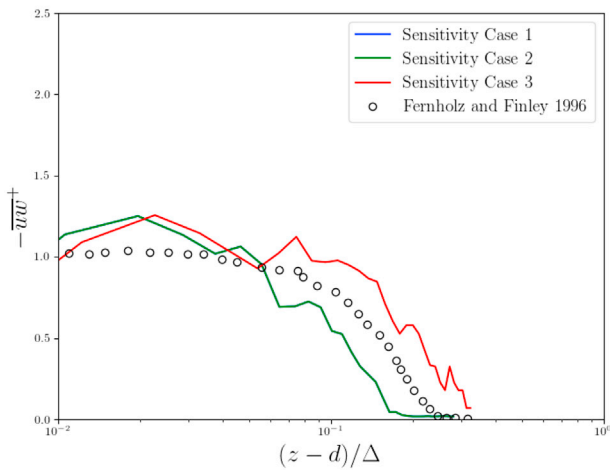
(b) Mean Horizontal Velocity Defect



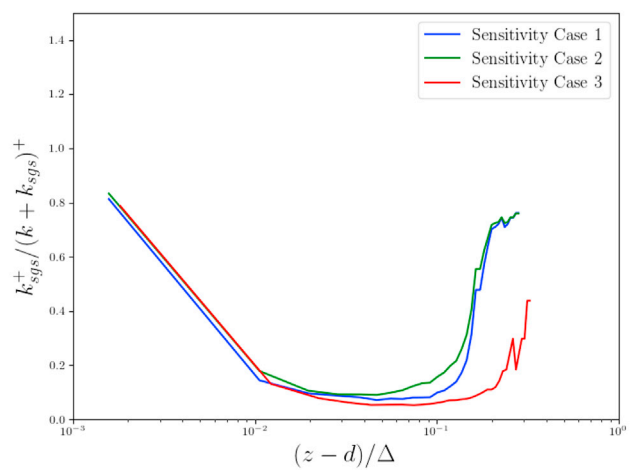
(c) Horizontal Velocity Variance



(d) Vertical Velocity Variance



(e) Reynolds Stress



(f) TKE Ratio

Fig. 4. Sensitivity of turbulence statistics to a_σ . Results for grid level III and profile 4 are presented for Case 1 ($a_\sigma = 0.1$), Case 2 ($a_\sigma = 0.2$), and Case 3 ($a_\sigma = 0.3$).

For the turbulent viscosity, the zero-gradient condition is used at the inlet and outlet. At the wall two conditions are possible, either zero-gradient for wall-resolving simulations (smooth walls) or the `nutkAtm-RoughWallFunction` boundary condition for rough surfaces. This condition modifies the turbulent viscosity near the surface such that

$$\nu_T = \nu \left(\frac{z^+ \kappa}{\ln \bar{E}} - 1 \right), \quad (25)$$

where, $z^+ = u_\tau z / \nu$ is the non-dimensional wall-normal distance, and $\bar{E} = (z + z_0) / z_0$.

2.5.3. Finite volume schemes

A second-order implicit backward time scheme is used, and all gradient schemes are based on second-order Gaussian integration with linear interpolation. All Laplacian schemes are based on corrected Gaussian integration with linear interpolation, which provides an unbounded, second order, and conservative numerical behaviour. Divergence schemes are based on Gaussian integration with linear or upwind interpolation, depending on the variable of interest (Greenshields, 2015).

2.5.4. Finite volume solution control

Throughout all simulations, timesteps are chosen so that the maximum Courant number satisfies $Co = \Delta t |\bar{U}| / \Delta x < 1$. The pressure matrix is preconditioned by the diagonal incomplete Cholesky technique and solved by the preconditioned conjugate gradient solver. Other variables are preconditioned by the diagonal incomplete-lower-upper technique and solved by the preconditioned bi-conjugate gradient solver. The pressure-linked equations (i.e. equations that have a pressure term) are solved by a hybrid method consisting of two algorithms: 1) the pressure-implicit split-operator method, and 2) the semi-implicit method (Greenshields, 2015).

2.5.5. Solution averaging

Once the flow passes over the domain in the streamwise direction, the simulations are extended for an additional twenty flow passes over the domain to obtain statistical information by time averaging. Note that one pass can be interpreted as the characteristic flow time in the streamwise direction and multiple characteristic flow times must be considered to obtain statistical information about the flow. In addition, instantaneous solutions are saved at every timestep in selected portions of the domain, including vertical lines (profiles) at various streamwise distances (Fig. 1) for further calculations.

2.6. Validation dataset

Wind tunnel flow experiments and other LES models are used to validate the VLES model developed in this study. For the smooth-wall condition, the datasets from Fernholz and Finley (1996) and Krogstad and Efros (2012) are used. For the rough-wall condition, the datasets from Cheng and Castro (2002) and Amir and Castro (2011) are used, where various roughness structures such as grits, blocks, and meshes were attempted. The subset considered in this study includes the blocks with characteristic aerodynamic roughness height of $z_0 = 0.0005$ m. Mean momentum or turbulence statistics are non-dimensionalized with friction velocity u_τ . Normal distance to the wall is typically non-dimensionalized using the friction velocity and fluid kinematic viscosity $(z - d)^+ = (z - d)u_\tau / \nu$. However, another convenient choice is $(z - d) / \Delta$, where d is displacement height and Δ , not to be confused with LES filter length, is the Clauser's scaling parameter defined as $\Delta = \delta^* U_e / u_\tau$. Here U_e is mean velocity on top of the boundary layer and δ^* is the displacement thickness (Aliabadi, 2018). The anisotropy of turbulence, as predicted by the VLES, is compared to LES results of Thomas and Williams (1999), where velocity variances in the x and z directions are analyzed vs. normal distance to the wall.

3. Results and discussion

The large eddy simulation is an incomplete turbulence model, for which grid convergence cannot be studied systematically (Roache, 1997; Poletto et al., 2013; Aliabadi, 2018). LES essentially formulates and solves different sets of partial differential equations at subgrid and above grid scales (Aliabadi et al., 2017). As a result, investigation of grid refinement and coarsening effects on the solutions should be performed in the form of a sensitivity study.

The main objective of a VLES model is to simulate mean properties of the flow, turbulence variances, and turbulence fluxes (covariances) accurately for coarse grids. Furthermore, spectral content of fluctuations and anisotropy may be desired to be partially simulated. This demands that a VLES model be tested and tuned on a series of grids from very fine to very coarse to ensure adequate performance. This is achieved in this study systematically.

First the VLES performance is assessed for wall-resolving simulations over the smooth surface. This allows testing the model for its synthetic and SGS parameterization, independent of wall functions, in a succession of coarse grids. Second, the VLES performance is assessed for rough-wall simulations using wall functions. In other words, the model is first tested by only coarsening interior grid cells while keeping the wall-adjacent cell height constant and then for its wall-function parameterization by only increasing the wall-adjacent cell height while keeping the interior cell resolution constant.

The turbulent boundary layer is characterized by a few bulk parameters. The important scaling parameter is the friction velocity u_τ , which is difficult to measure experimentally, especially for rough-wall experiments (Amir and Castro, 2011; Krogstad and Efros, 2012). For the LES results, friction velocity is determined in two ways. For wall-resolving simulations, friction velocity is determined by the fourth root of the sum of the squares of the shear components of Reynolds stress in the log-law range $u_\tau = (\overline{uw}^2 + \overline{vw}^2)^{1/4}$. This range itself is determined by specifying a lower and upper bound for z^+ . This method has been successfully implemented by Amir and Castro (2011). For rough-wall simulations with wall functions, for which the wall-adjacent cell includes the majority of log-law range, i.e. the volume of the wall-adjacent cell is large compared to most eddies with the consequence that the unresolved (i.e. parameterized) TKE outweighs the resolved TKE, we can additionally calculate friction velocity having the SGS TKE by $u_\tau = C_\mu^{1/4} k_{sgs}^{1/2}$. The turbulent boundary layer is further characterized by boundary-layer height δ , where mean streamwise velocity reaches 99% of freestream velocity, displacement thickness $\delta^*(x) \equiv \int_0^\infty \left(1 - \frac{\bar{U}(z)}{U_e}\right) dz$, momentum thickness $\theta(x) \equiv \int_0^\infty \frac{\bar{U}(z)}{U_e} \left(1 - \frac{\bar{U}(z)}{U_e}\right) dz$, momentum Reynolds number $Re_\theta = \theta u_\tau / \nu$, and the Clauser scaling parameter $\Delta = \delta^* U_e / u_\tau$.

3.1. Smooth surface wall-resolving simulations

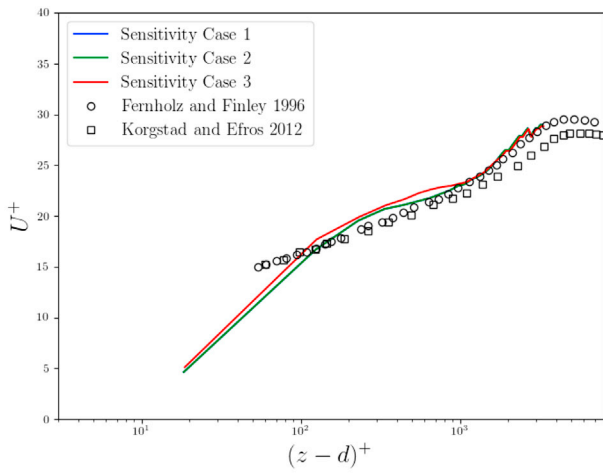
3.1.1. Model performance with grid coarsening

The model is first run with a choice of parameters describing inlet flow conditions suitable for a refined VLES. We set $U_{ref} = 1$ m s⁻¹, $z_{ref} =$

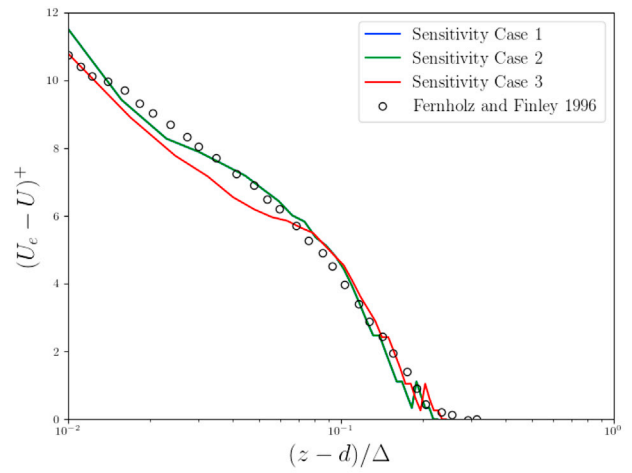
Table 4

Sensitivity of boundary-layer bulk features to a_τ for the smooth surface wall-resolving simulations. Grid level III is used and the results are provided for profile 4.

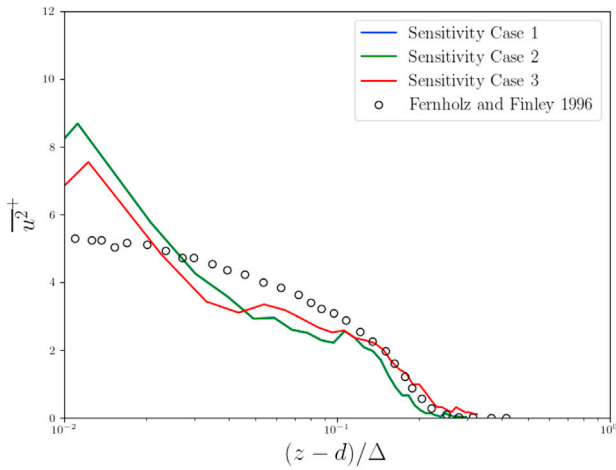
Constant	$a_\tau = 0.01$	$a_\tau = 0.05$	$a_\tau = 0.1$
u_τ [m s ⁻¹]	0.068	0.068	0.068
δ [m]	0.941	0.941	0.795
δ^* [m]	0.152	0.152	0.142
θ [m]	0.107	0.107	0.102
Re_θ	10,400	10,400	10,000
Δ [m]	3.44	3.44	3.30



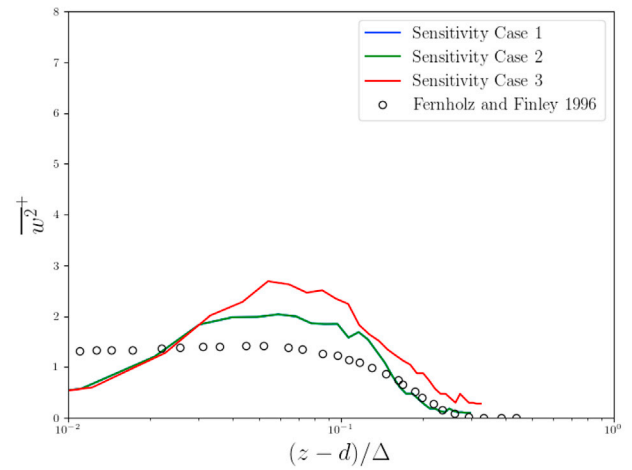
(a) Mean Horizontal Velocity



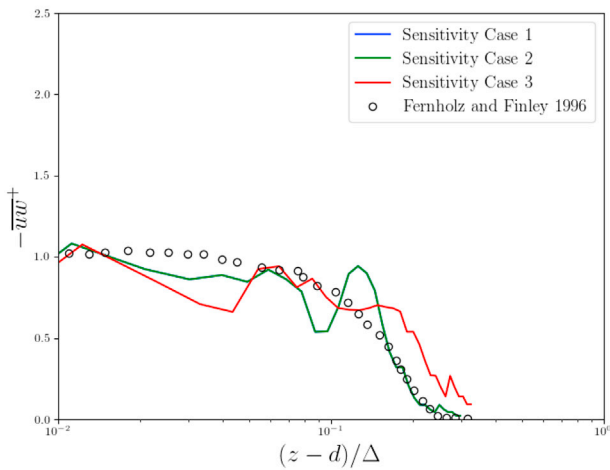
(b) Mean Horizontal Velocity Defect



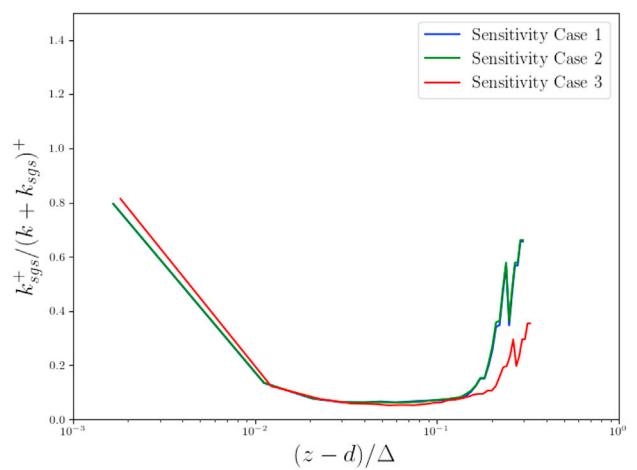
(c) Horizontal Velocity Variance



(d) Vertical Velocity Variance



(e) Reynolds Stress



(f) TKE Ratio

Fig. 5. Sensitivity of turbulence statistics to a_τ . Results for grid level III and profile 4 are presented for Case 1 ($a_\tau = 0.01$), Case 2 ($a_\tau = 0.05$), and Case 3 ($a_\tau = 0.1$).

0.1 m, power law exponent $\alpha = 0.189$, number of vortices at inlet $N = 200$, maximum turbulence intensity $I_{u,max} = 1$, parameter controlling energy-containing eddy or vortex size $a_\sigma = 0.2$, and parameter controlling energy-containing eddy or vortex lifetime $a_\tau = 0.01$. This choice of a_σ ensures that characteristic length of energy-containing eddies is greater than the coarsest grid size, i.e. $\ell_0 > \Delta$. The choice of a_τ , however, is made so that eddy lifetime for all vortices is in the order of model timestep. The choice of these important two parameters will be later investigated in Sect. 3.1.2.

Table 2 shows the simulated boundary-layer bulk features as a function of grid level. A range of values are provided for each feature as was monitored for profiles 1 to 4. A high level of agreement is maintained for all bulk features for grid levels I, II, and III; however, for grid level IV, although the friction velocity u_τ and Clauser's scaling parameter Δ are preserved, the boundary layer height δ , displacement thickness δ^* , momentum thickness θ , and momentum Reynolds number Re_θ are underestimated. Therefore, grid level III is the coarsening limit for preserving the boundary-layer bulk features.

Fig. 2 shows the non-dimensionalized horizontal mean velocity vs. non-dimensionalized wall-normal distance for different grid levels. It can be seen that log-law of the wall can be produced in good agreement with observations for grid levels I, II, and III. Also it can be seen that the adaptation distance is in the order of 4δ so that even though profiles 1 – 3 may not agree with the experiments, profile 4 agrees with the experimental observations. For grid level IV, neither the log-law of the wall is produced, nor is the model in agreement with experimental observations.

Fig. 3 shows various non-dimensionalized turbulence statistics vs. non-dimensionalized wall-normal distance using the Clauser scaling parameter for grid level III. For brevity, the statistics were also obtained for other grid levels, but the graphical results are not shown. The comparison of the statistics among different grid levels confirms that grid level III is the coarse limit for the VLES model with the current settings.

For non-dimensionalized horizontal velocity variance vs. non-dimensionalized wall-normal distance for different grid levels, the model vs. experimental agreement is reasonable, except for grid level IV. The adaptation distance for this turbulence statistic is 2δ as can be seen the variance is significantly overestimated on profile 1. The variance is maintained throughout the length of the domain such that the turbulence is not decaying downstream from the inlet, where it is seeded by the imposed vortices.

For non-dimensionalized vertical velocity variance vs. non-dimensionalized wall-normal distance for different grid levels, the model vs. experimental agreement is reasonable, except for grid level IV although all simulations slightly overestimate this variance in the mid height of the channel. The adaptation distance for this turbulence statistic is 4δ as can be seen the variance is significantly overestimated on profile 1 but drops for profiles 2, 3, and 4. The variance is maintained throughout the length of the domain.

For non-dimensionalized Reynolds stress vs. non-dimensionalized wall-normal distance for different grid levels, the model vs. experimental agreement is reasonable, except for grid level IV. The adaptation distance for this turbulence statistic is also 4δ . As can be seen the Reynolds stress is significantly overestimated on profile 1 but drops for profiles 2, 3, and 4. This statistic is also maintained throughout the length of the domain. The analysis of the variances and Reynolds stress reveals that the VLES model can successfully reproduce experimental observations on grid levels I, II, and III.

For non-dimensionalized total TKE, SGS and resolved, vs. non-dimensionalized wall-normal distance for different grid levels, the profiles exhibit similarity with the two variances presented. Again, it is confirmed that the adaptation distance is about 2δ . In addition, grid levels I, II, and III produce similar results.

An important attribute of any LES model is the ratio of the TKE modelled by the simulation, i.e. k_{sgs} , to the total TKE modelled and resolved by the simulation, i.e. $k + k_{sgs}$. For models based on the

Smagorinsky (1963) or WALE (Fröhlich et al., 2005) SGS closure schemes, a ratio is reported using the residual viscosity divided by the molecular viscosity. The higher the ratio is in a particular space and time in the domain, the more the TKE is modelled and the less it is resolved. For our simulation, fortunately, both k_{sgs} and k are available. The former is a solution of the model and the latter can be obtained by post processing. Therefore, we obtain the ratio of the modelled to the total TKE. It can be seen that near the wall and the top of the domain more of the TKE is modelled; however, in the interior it is significantly resolved. It appears that for a successful VLES, at most 20% of the TKE in the interior of the domain shall be modelled and more than 80% shall be resolved. This criteria can be seen for grids levels, I, II, and III, where good agreement between the model and experimental observations was reached.

3.1.2. Sensitivity to a_σ and a_τ

The sensitivity of the numerical solution to a_σ is investigated on grid level III and on profile 4. Table 3 shows the simulated boundary-layer bulk features as a_σ varies from 0.1 to 0.3. It can be seen that most bulk features are approximately preserved regardless of the value of a_σ except for Clauser's scaling parameter.

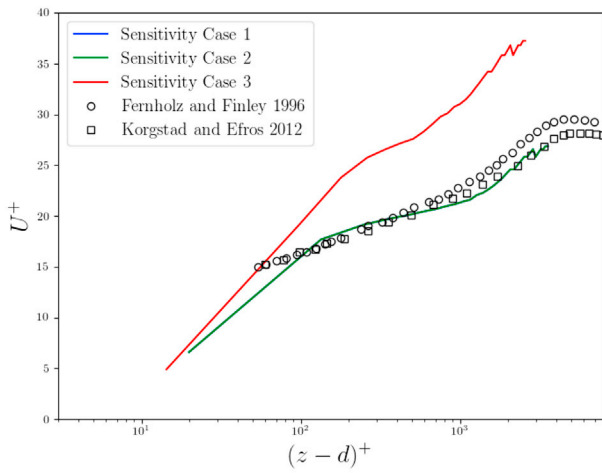
Fig. 4 shows the sensitivity of the turbulence statistics on grid level III and profile 4. Variation in a_σ does not influence mean horizontal velocity and horizontal velocity variance substantially. However, increasing a_σ shifts the curves for vertical velocity variance and Reynolds stress to the right. This can be understood as feeding larger vortices or eddies at the inlet will result in greater fluctuations in the resolved scales away from the wall. Increasing a_σ will also reduce the ratio of modelled to total TKE away from the wall. This is evident as feeding larger eddies to the flow will cause more TKE to be resolved.

The sensitivity of the numerical solution to a_τ is investigated on grid level III and on profile 4. Table 4 shows the simulated boundary-layer bulk features as a_τ varies from 0.01 to 0.1. It can be seen that most bulk features are approximately preserved regardless of the value of a_τ except for the boundary layer height.

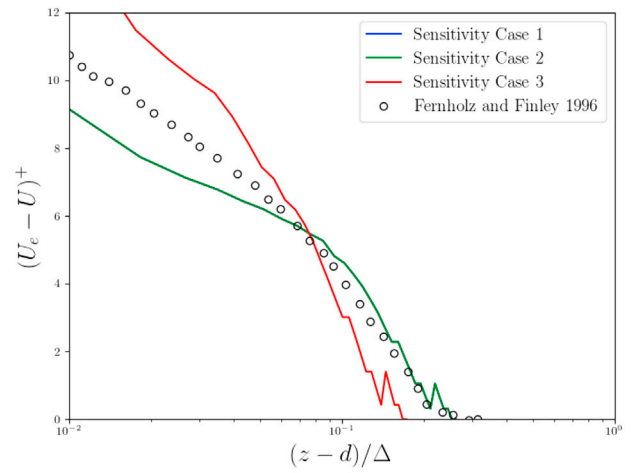
Fig. 5 shows the sensitivity of the turbulence statistics on grid level III and profile 4. Variation in a_τ does not influence mean horizontal velocity or horizontal velocity variance substantially. However, increasing a_τ shifts the curves for vertical velocity variance upward and the curve for Reynolds stress to the right. It appears that the suitable eddy lifetime is one in which $a_\tau = 0.01$, i.e. a value of a_τ that results in a lifetime equal to the timestep of the model. Estimating an optimal eddy timescale is a non-trivial exercise requiring a sensitivity analysis. The optimal timescale is determined by the complex two-way interaction between the inner and outer boundary layers (Raupach et al., 1991). On the one hand, vortices and instabilities at large scale in the outer region break down the energy cascade, so it may seem a large eddy lifetime at the inlet is desirable. On the other hand, vortices and instabilities are generated near the wall and grow into the outer layer, so it may seem a small eddy lifetime at the inlet is desirable. This reasoning is suggested because the model simulates both processes. It is revealed by this sensitivity analysis that a small eddy lifetime results in a solution giving closer agreement with experimental observations.

Table 5
Sensitivity of boundary-layer bulk features to C_Δ for the smooth surface wall-resolving simulations. Grid level III is used and the results are provided for profile 4.

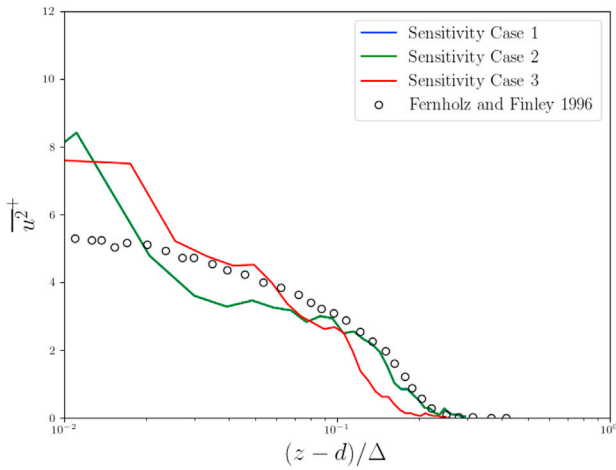
Constant	$C_\Delta = 0.5$	$C_\Delta = 1$	$C_\Delta = 1.5$
u_τ [m s ⁻¹]	0.068	0.068	0.068
δ [m]	0.941	0.941	0.941
δ^* [m]	0.152	0.152	0.154
θ [m]	0.107	0.107	0.106
Re_θ	10,400	10,400	10,200
Δ [m]	3.44	3.44	3.82



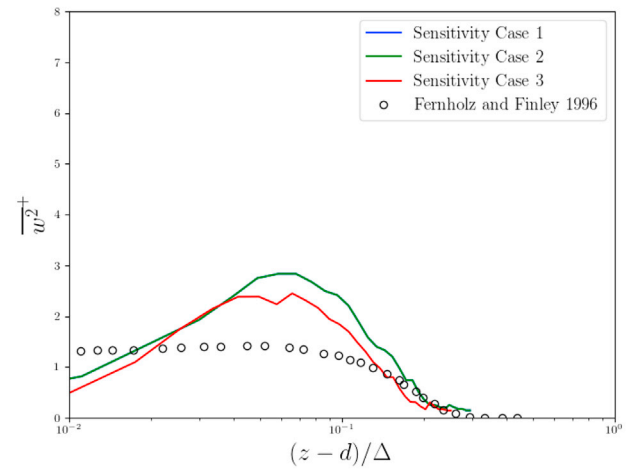
(a) Mean Horizontal Velocity



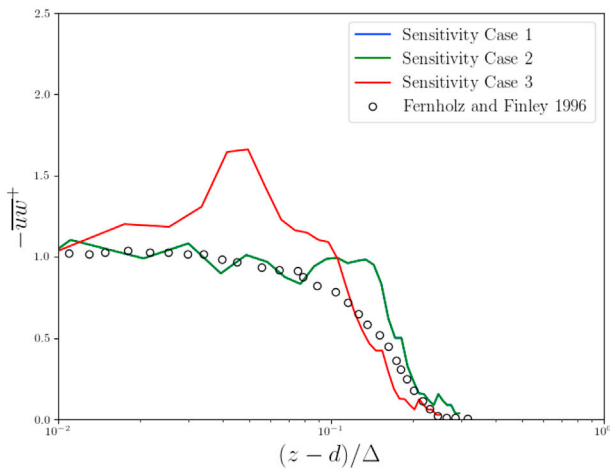
(b) Mean Horizontal Velocity Defect



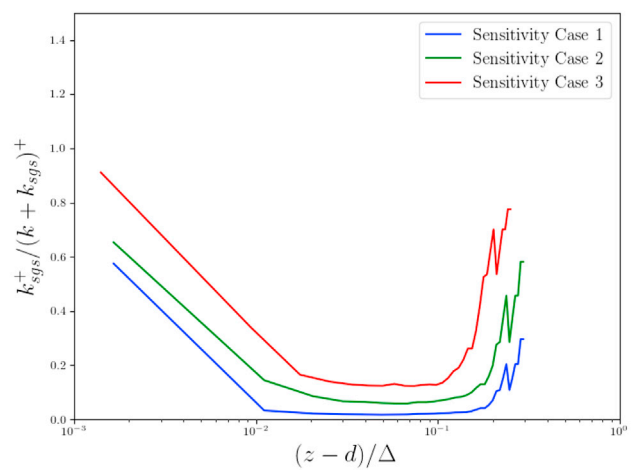
(c) Horizontal Velocity Variance



(d) Vertical Velocity Variance

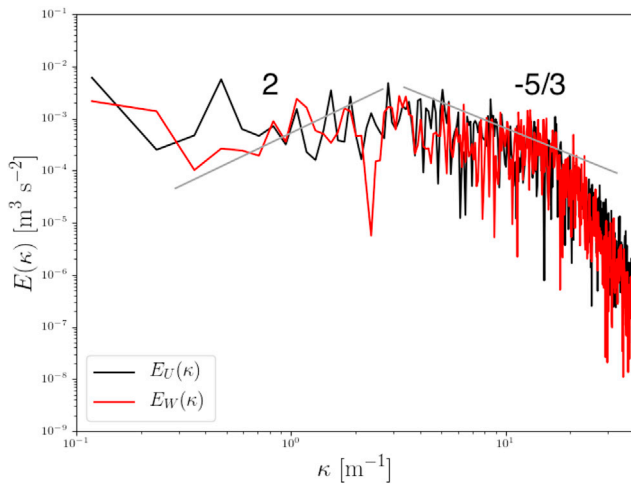


(e) Reynolds Stress

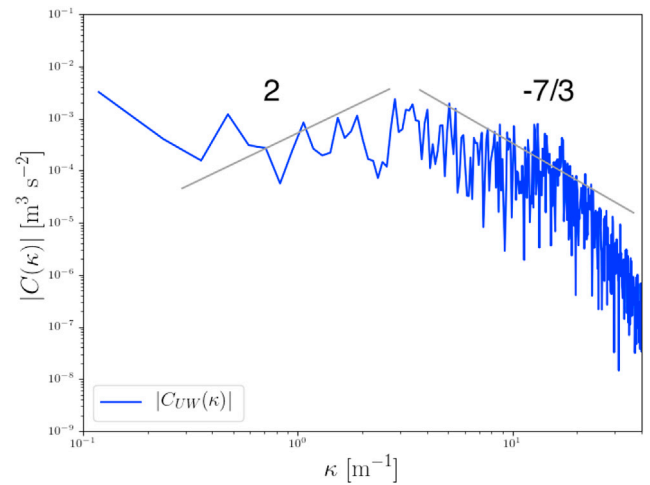


(f) TKE Ratio

Fig. 6. Sensitivity of turbulence statistics to C_{Δ} . Results for grid level III and profile 4 are presented for Case 1 ($C_{\Delta} = 0.5$), Case 2 ($C_{\Delta} = 1$), and Case 3 ($C_{\Delta} = 1.5$).



(a) Spectral Energy



(b) Co-spectral Energy

Fig. 7. Spectral and co-spectral energies for wall-resolving simulations for grid level III, profile 4, and $z - d = z_{ref}$.

3.1.3. Sensitivity to C_Δ

The sensitivity of the SGS model is tested by varying constant C_Δ that controls the SGS lengthscale l . The default value for C_Δ was 1 in the previous simulations, but here it is varied to 0.5 and 1.5 as well. Table 5 shows the simulated boundary-layer bulk features as a function of varying C_Δ . The boundary-layer properties are preserved for $C_\Delta = 0.5$ although there are slight variations for $C_\Delta = 1.5$.

Fig. 6 shows the sensitivity of the turbulence statistics on grid level III and profile 4. Unlike previous sensitivity tests, variations in C_Δ does influence mean horizontal velocity substantially. Particularly, with greater value of $C_\Delta = 1.5$ the mean velocity is overpredicted. Although the horizontal and vertical velocity variances are slightly underpredicted with $C_\Delta = 1.5$, the effect of increasing C_Δ on the magnitude of the Reynolds stress is unclear. The ratio of modelled to total TKE is evidently controlled by C_Δ . The higher the C_Δ , the more dissipative the SGS model and the greater the portion of the TKE that is modelled, although to the limit of about 20% for the model interior for these simulations. It appears

that the relative strength of the SGS model dissipation can be successfully controlled by the choice of C_Δ .

Of course, other SGS model parameters could have been tested in a sensitivity study, such as C_k or C_e . However, for brevity of the current analysis, and for practicality of only resorting to a few adjustable constants in this VLES model, only C_Δ is studied and proposed to be adjusted for the model, potentially for other flow applications.

3.1.4. Spectral analysis for wall-resolving simulations

LES models are frequently benchmarked using spectral analysis to investigate if they can resolve the inertial subrange or the combination of energy-containing and the inertial subranges (Thomas and Williams, 1999; Huang et al., 2010; Castro and Paz, 2013; Aboshosha et al., 2015b; Ricci et al., 2017). For both isotropic and anisotropic turbulence (e.g. the atmosphere), it has been suggested that in the inertial subrange, the slope of the energy spectrum density $E(k)$ for velocity fluctuations in all directions versus the wavenumber k in the log-log scale is $-5/3$

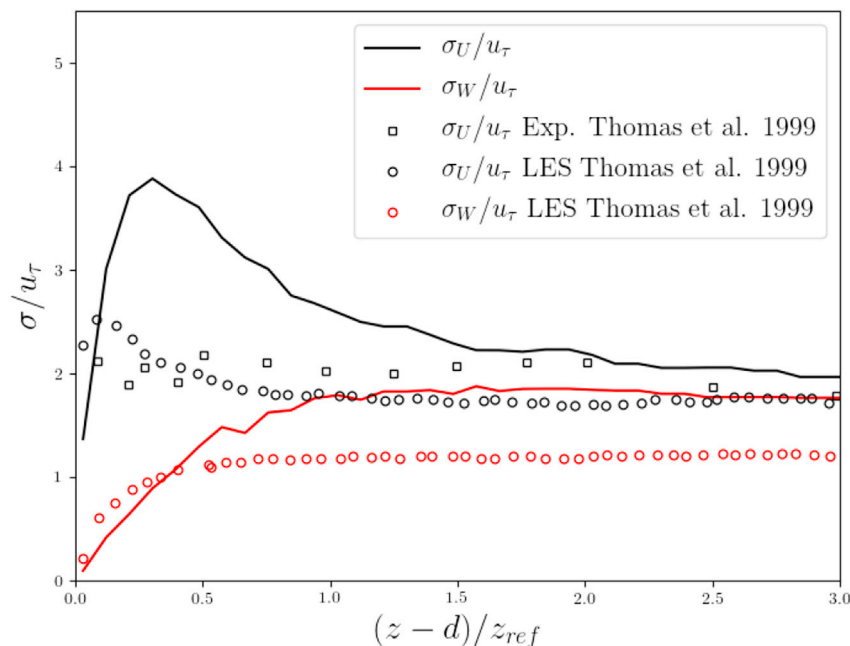
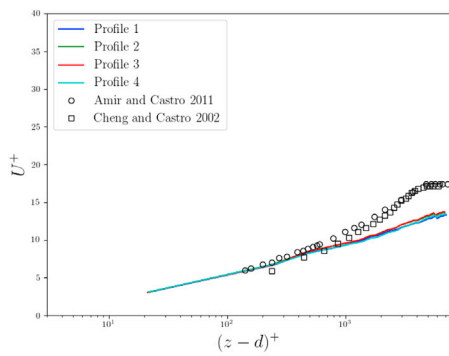
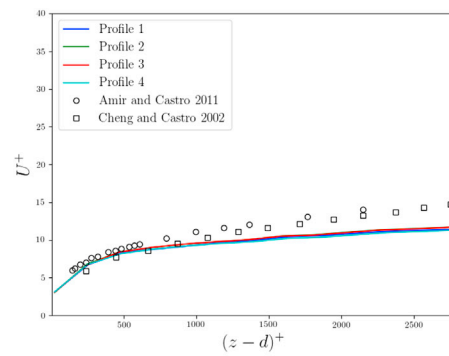


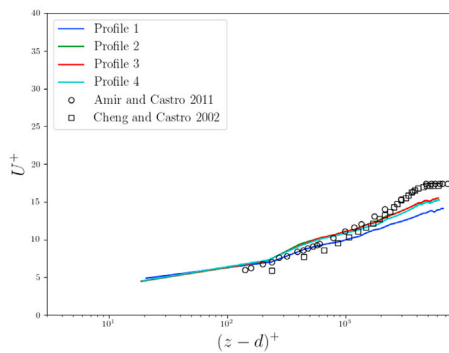
Fig. 8. Profiles of velocity component variances in the x and z directions for grid level III, and profile 4.



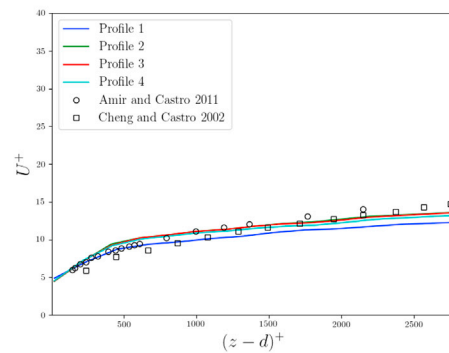
(a) $(z - d)^+ = 44.5 - 46.9$



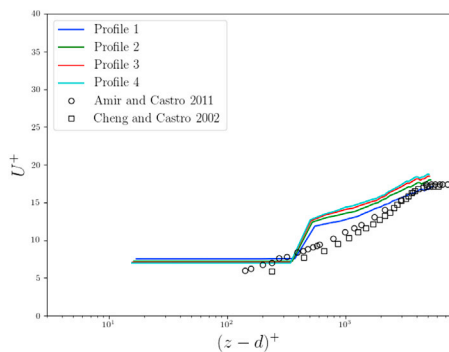
(b) $(z - d)^+ = 44.5 - 46.9$



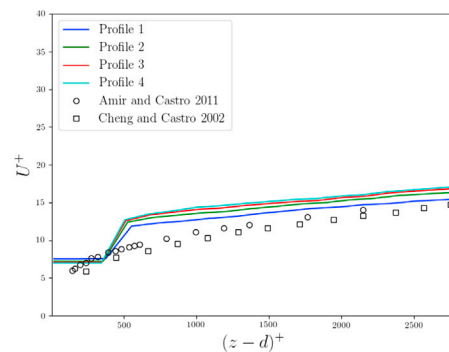
(c) $(z - d)^+ = 81.7 - 92.0$



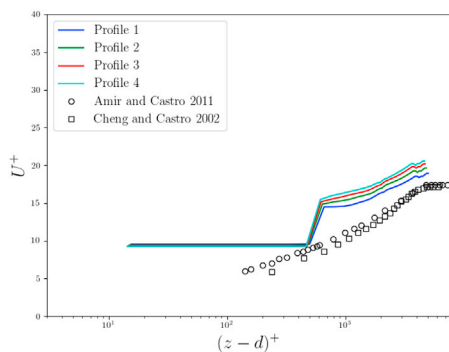
(d) $(z - d)^+ = 81.7 - 92.0$



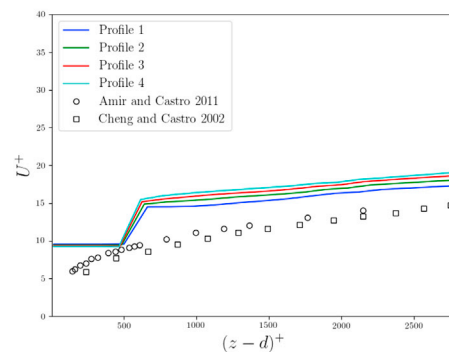
(e) $(z - d)^+ = 133 - 151$



(f) $(z - d)^+ = 133 - 151$



(g) $(z - d)^+ = 144 - 188$



(h) $(z - d)^+ = 144 - 188$

Fig. 9. Non-dimensional horizontal mean velocity vs. non-dimensional wall-normal distance for different $(z - d)^+$ in the mid height of the first computational cell in both logarithmic (a, c, e, g) and linear (b, d, f, h) scales.

(Kolmogorov spectrum) (Kaimal et al., 1972, 1976; Pope, 2000). It has been suggested that for anisotropic atmospheric flows, and in the inertial subrange, the slope of the co-spectral density $C(\kappa)$ for velocity fluctuations along streamwise (x) and vertical (z) directions versus the wave-number κ in the log-log scale is approximately $-7/3$ (Kaimal et al., 1972). It has also been suggested that the slope in the energy-containing subrange for spectral $E(\kappa)$ and co-spectral $C(\kappa)$ densities of most variables in anisotropic atmospheric flows is approximately 2 (Kaimal et al., 1972, 1976), while it is approximately 4 for other isotropic flows (von Kármán, 1948; Pope, 2000). For the present analysis, a discrete Fourier transform is used to calculate the spectra that are subsequently transformed into spectral density by dividing with the wave number bin width (Stull, 1988). The wave number is estimated using Taylor's hypothesis (Taylor, 1938) $\kappa = 2\pi n/(P\bar{U})$, where n is the number of cycles in the time period of analysis P and \bar{U} is time-averaged velocity component along the flow (Kaimal et al., 1976; Aliabadi, 2018). The spectral and co-spectral densities are calculated for the wall-resolving case, grid level III, profile 4, and $z - d = z_{ref}$.

Fig. 7a shows the spectral content of turbulence resolved by the VLES. The resolved range covers more than two orders of magnitude of wave numbers. For comparison to model spectra, the inertial subrange and the energy-containing subrange slopes ($-5/3, 2$) are also shown in the figure. For the spectral energy, the inertial subrange is partially matched in agreement with other LES models of the same caliber (See Figs. 8 and 9 in Thomas and Williams (1999), Fig. 17 in Aboshosha et al. (2015a), Fig. 7 in Ricci et al. (2017)), while smaller scales of the inertial subrange are modelled (not resolved) resulting in the sharp drop and truncation of the spectra. In comparison, other LES models resolve a greater portion of the inertial subrange or do not show the unresolved portions (See Figs. 3, 8, and 15 in Huang et al. (2010), Figs. 2 and 12 in Castro and Paz (2013), Figs. 3, 6, and 18 in Aboshosha et al. (2015b), Figs. 8, 13, 14, 15, and 16 in Castro et al. (2017)). In agreement with these results, for anisotropic turbulence, most LES studies report a slope much less than 2 for the energy-containing subrange (Thomas and Williams, 1999; Huang et al., 2010; Castro and Paz, 2013; Aboshosha et al., 2015b; a; Castro et al., 2017; Ricci et al., 2017).

LES models are commonly analyzed to simulate coherency. Coherency is essentially a normalized amplitude, and is a real number in the range 0 and 1. It acts similar to frequency-dependent correlation coefficient and can be defined for any two velocity components, say U and W (Stull, 1988; Castro et al., 2017). Alternative to coherency, we have analyzed the co-spectral density $C(\kappa)$, which is a representation of frequency-dependent correlation between pairs of velocity component fluctuations. As shown in Fig. 7b, the co-spectral density shows higher activity and thus correlation for lower wave numbers, in reasonable agreement with studies reporting coherency of LES models (Aboshosha et al., 2015b; Castro et al., 2017). For comparison to model spectra, the inertial subrange and the energy-containing subrange slopes ($-7/3, 2$) are also shown in the figure. The expected slope in the inertial subrange is partially matched.

It must be noted that given the simplistic nature of the VLES model, there is neither further analysis nor any expectation for a precise simulation of coherent structures or spectral content in the flow in comparison to other advanced synthetic methods.

3.1.5. Anisotropy for wall-resolving simulations

In this study anisotropy is considered in the context of velocity component variances along the x and z directions. Fig. 8 shows the profiles of velocity component variances compared to wind tunnel experiments and LES model of Thomas and Williams (1999) who used the power law method for inlet wind speed with the same z_{ref} and a similar α . Although a direct comparison is difficult, at $z - d = z_{ref}$, the VLES model ($\sigma_U/\sigma_W = 1.5$) is in good agreement with LES results of Thomas and Williams (1999) ($\sigma_U/\sigma_W = 1.5$). This result indicates that the VLES model simulates the anisotropy of the boundary layer turbulence reasonably well.

3.2. Rough-wall simulations with wall functions

3.2.1. Sensitivity to $(z - d)^+$

To study the effect of wall functions for rough-wall simulations, grid level III is chosen for further analysis because it provided solutions acceptably close to grid levels I and II but at significantly lower computational cost. It was found that the best agreement with experimental observations were achieved when $a_\sigma = 0.2$ and $a_\tau = 0.5$. In other words, larger eddy time scales had to be assumed compared to wall-resolving simulations ($a_\tau = 0.01$) for more accurate results. This can be explained by the fact that when wall functions are used, turbulence generation near the walls is modelled as opposed to resolved, in which case eddy formation at some distance away from the wall occurs with a larger time constant. This implies that TKE transfer from the wall to the outer layer starts with larger time constants, and therefore, it necessitates more model timestep iterations before new eddies are sampled at the inlet.

Four simulations are conducted by varying the height of the first computational cell, for which a $(z - d)^+$ is calculated using z associated with the mid height of first computational cell z_p . Table 6 shows the simulated boundary-layer bulk features as a function of $(z - d)^+$. It can be observed that friction velocity gradually declines by increasing $(z - d)^+$. The boundary-layer height, displacement thickness, and momentum thickness are preserved for the four simulations. In addition the momentum Reynolds number is preserved. The Clauser's scaling parameter gradually increases by increasing $(z - d)^+$.

Fig. 9 shows the non-dimensionalized horizontal mean velocity vs. non-dimensionalized wall-normal distance for different computational grids and the associated $(z - d)^+$ for the first layer of cells adjacent to the wall. It can be seen that log-law of the wall can be produced in good agreement with observations for smaller values of $(z - d)^+$. On the other hand, the edge of the outer layer is better produced when $(z - d)^+$ becomes larger. Also it can be seen that the adaptation distance is in the order of boundary-layer height δ . The horizontal or flat portion of the solution belongs to the first computational cell, in which the volume-averaged solution is represented. The flat portion of the curves increase by increasing $(z - d)^+$. The largest range of values for $(z - d)^+$ indicate that the velocity is over-predicted in both the log-law region and the edge of the outer layer. This phenomenon will be discussed at the end of this section.

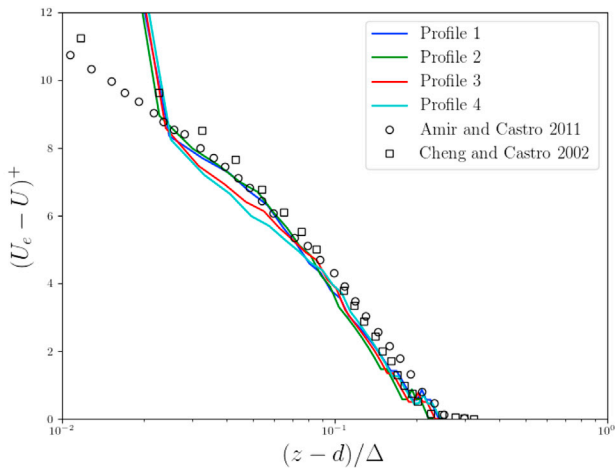
Fig. 10 shows various non-dimensionalized turbulence statistics vs. non-dimensionalized wall-normal distance using the Clauser scaling parameter for the level of first layer of grid cells coarseness associated with $(z - d)^+ = 133 - 151$. For brevity, the statistics were also obtained for other first layer of grid cells coarseness, but the graphical results are not shown.

For non-dimensionalized horizontal velocity variance vs. non-dimensionalized wall-normal distance for different $(z - d)^+$ in the mid height of the first computational cell, the model vs. experimental agreement is reasonable, although in all cases the variance is under-predicted for the greater portion of the model interior. Nevertheless, the trend is reproduced and turbulence is maintained within the domain. The adaptation distance for this turbulence statistic is 2δ .

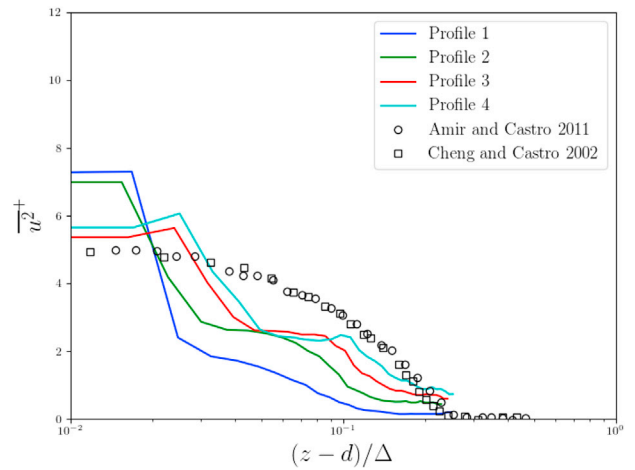
Table 6

Boundary-layer bulk features for rough-wall simulations while coarsening the first layer of computational cells adjacent to the wall. For each grid $(z - d)^+$ is calculated using the mid height of the first computational cell adjacent to the wall. The range of results are provided for profiles 1, 2, 3, and 4.

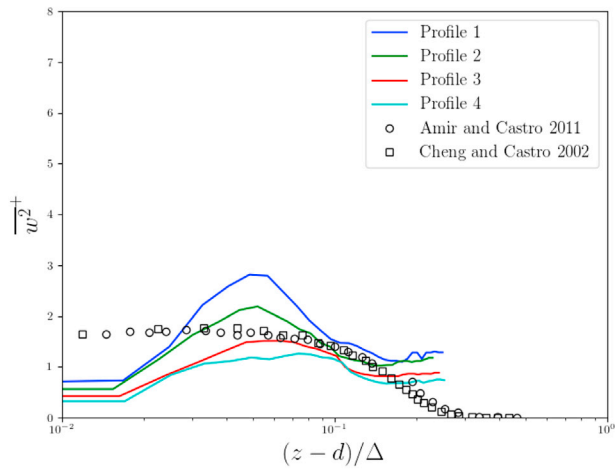
$(z - d)^+$	44.5–46.9	81.7–92.0	133–151	144–188
u_τ [m s ⁻¹]	0.112–0.116	0.099–0.109	0.083–0.090	0.075–0.081
δ [m]	0.795–0.941	0.800–0.941	0.804–0.804	0.809–0.809
δ^* [m]	0.146–0.154	0.146–0.155	0.146–0.153	0.144–0.148
θ [m]	0.101–0.105	0.102–0.105	0.103–0.103	0.101–0.102
Re_θ	9700–10,100	9800–10,100	9900–1000	9800–9900
Δ [m]	3.06–3.32	3.05–3.63	3.92–4.32	4.58–5.78



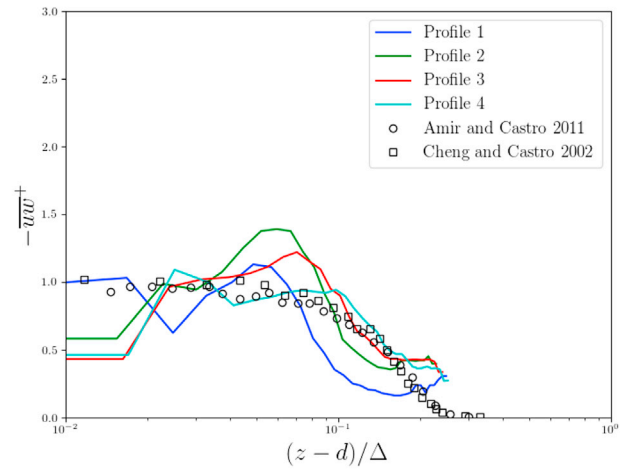
(a) Mean Horizontal Velocity Defect



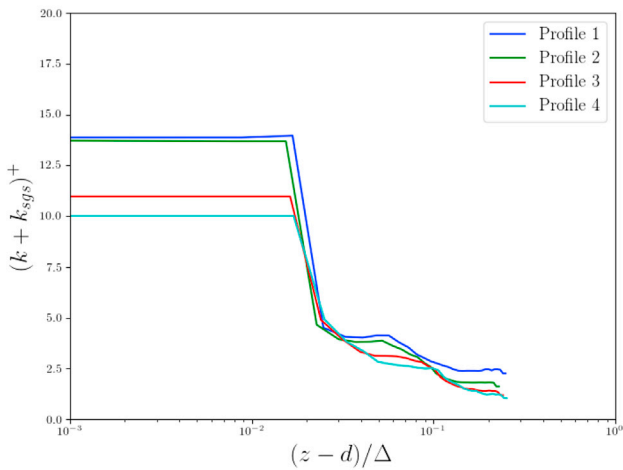
(b) Horizontal Velocity Variance



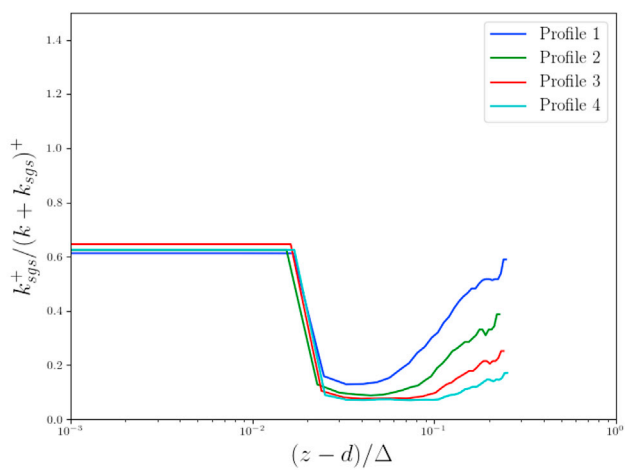
(c) Vertical Velocity Variance



(d) Reynolds Stress



(e) Total TKE



(f) TKE Ratio

Fig. 10. Non-dimensionalized turbulence statistics vs. non-dimensionalized wall-normal distance using the Clauser parameter for grid level III, where $(z - d)^+ = 133 - 151$, based on the mid height of the first computational cell.

For non-dimensionalized vertical velocity variance vs. non-dimensionalized wall-normal distance for different $(z - d)^+$ in the mid height of the first computational cell, the model vs. experimental agreement is reasonable, except for the largest range of $(z - d)^+$. This variance increases gradually by increasing $(z - d)^+$. All simulations underestimate this variance closer to the wall. The adaptation distance for this turbulence statistic is 2δ . The variance is maintained throughout the length of the domain.

For non-dimensionalized Reynolds stress vs. non-dimensionalized wall-normal distance for different $(z - d)^+$ in the mid height of the first computational cell, the model vs. experimental agreement is reasonable for the lower of the two ranges of $(z - d)^+$ although the disagreement increases for the larger range of $(z - d)^+$. The adaptation distance for this turbulence statistic is also 2δ . This statistic is also maintained throughout the length of the domain.

For non-dimensionalized total TKE, SGS and resolved, vs. non-dimensionalized wall-normal distance for different $(z - d)^+$, the profiles exhibit similarity for the first three ranges of $(z - d)^+$, however, for the largest $(z - d)^+$ range, the profiles do not overlap, indicating that turbulence has not reached a statistically stationary condition downstream of the tunnel. For the first three ranges of $(z - d)^+$ the adaptation distance is about 2δ .

For ratio of the modelled to the total TKE, it can be seen that near the wall and the top of the domain more of the TKE is modelled; however, in the interior it is significantly resolved. Again, it appears that for a successful VLES, at most 20% of the TKE in the interior of the domain shall be modelled and more than 80% shall be resolved.

The upper limit for $(z - d)^+$, to lie in the log-law regime, has been reported to be in the range 500 – 1000 (Blocken et al., 2007) and even as high as 10000 (to be nearly in the log-law regime) (Kays and Crawford, 1993). The fundamental question is whether the current VLES model should produce the same quality of results using a wall function based on the log-law when $(z - d)^+$ is further increased to values suggested in the literature as the upper limit. As is found here, the results start to show deviation from experiments when $(z - d)^+$ is increased. However, this finding is not conclusive and cannot be generalized to deem the VLES model a successful or an unsuccessful model for a particular practical application. The following reasons can be stated. 1) With the current simulation setup, the thickness of the first layer of computational mesh quickly grows to occupy a significant depth of the boundary layer. For instance for $(z - d)^+ = 144 - 188$ the thickness of the first layer of

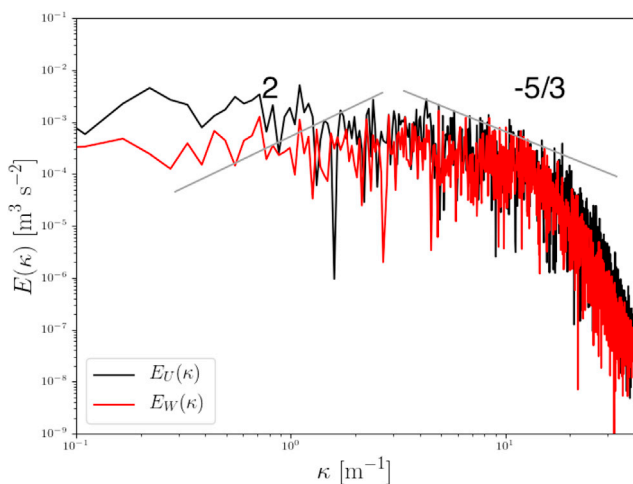
computational mesh is already more than 10% of the boundary-layer depth δ . This is unrealistic for practical applications of the VLES model. For the same reason, the same simulation model cannot be tested for larger values of $(z - d)^+$. 2) The height of the simulated boundary layer limits the largest size of eddies that can exist in the domain, with implications in reducing turbulent mixing lengths in comparison to real atmospheric conditions, particularly if eddies are not generated near the walls using wall-resolving simulations. This phenomenon has been reported to artificially overpredict mean wind speeds compared to experiments when wall functions are used in LES (Thomas and Williams, 1999). This is in agreement with our study that also overpredicts mean wind speeds when using larger values of $(z - d)^+$ (See Fig. 9). 3) Wall functions can be carefully calibrated or aggregated for a variety of roughness length scales, roughness structure geometries, and plan or frontal area densities (Jiménez, 2004; Blocken et al., 2007; Anderson and Meneveau, 2010; Kent et al., 2017). For this reason, the current VLES model shall be tested on larger domains for problems involving practical applications with an attempt to modify or adjust wall functions to deem successful or unsuccessful results.

3.2.2. Spectral analysis for rough-wall simulations

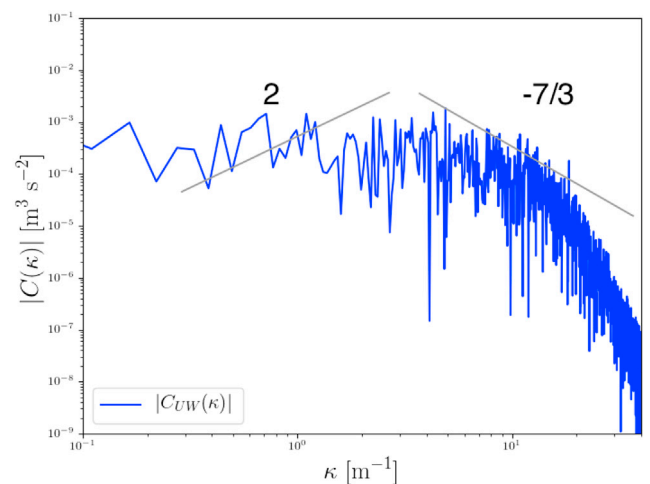
Similar to the wall-resolving simulations, for rough-wall simulations, the spectral and co-spectral densities are calculated for the case with $(z - d)^+ = 133 - 151$, profile 4, and $z - d = z_{ref}$. Fig. 11 shows the spectral and co-spectral content of turbulence resolved by the VLES. The findings are similar to the wall-resolving simulation case, with no loss of spectral content as a result of using wall functions. This justifies the use of wall-functions for the VLES model to reduce the computational cost.

3.2.3. Anisotropy for rough-wall simulations

Similar to the wall-resolving simulations, for rough-wall simulations, the anisotropy of turbulence is analyzed using velocity variances along the x and z directions. Fig. 12 shows the profiles of velocity component variances compared to the results of Thomas and Williams (1999) for a similar flow. At $z - d = z_{ref}$, the VLES model ($\sigma_U/\sigma_W = 2.5$) is in less agreement with LES results of Thomas and Williams (1999) ($\sigma_U/\sigma_W = 1.5$); however the agreement is still good further away from the wall. Nevertheless, the VLES model still predicts $\sigma_U > \sigma_W$ in all regions away from the wall. This result indicates that the VLES model simulates the anisotropy of the boundary layer turbulence less accurately near the wall but with the benefit of lowering the computational cost.



(a) Spectral Energy



(b) Co-spectral Energy

Fig. 11. Spectral and co-spectral energies for rough-wall simulations for the case with $(z - d)^+ = 133 - 151$, profile 4, and $z - d = z_{ref}$.

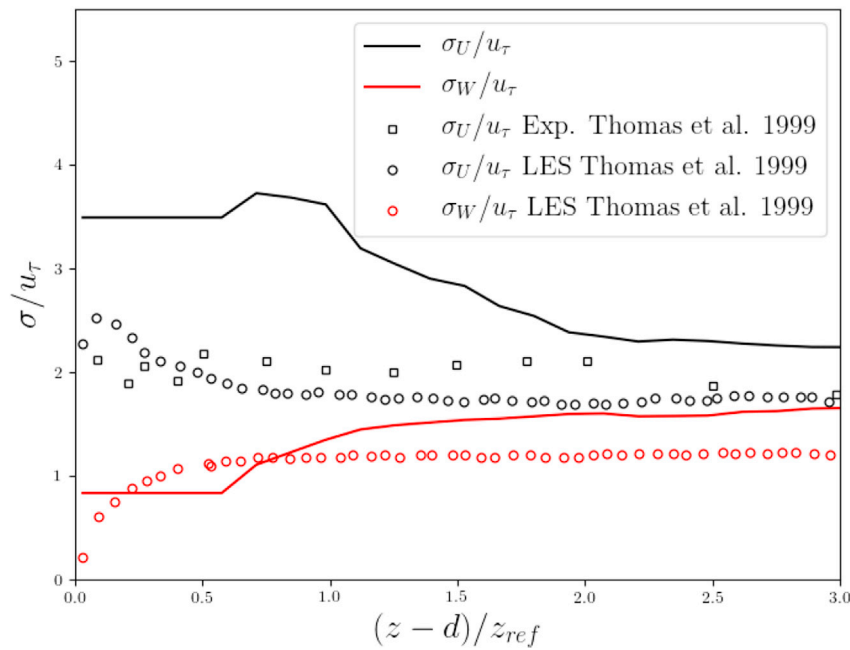


Fig. 12. Profiles of velocity component variances in the x and z directions for the case with $(z - d)^+ = 133 - 151$ and profile 4.

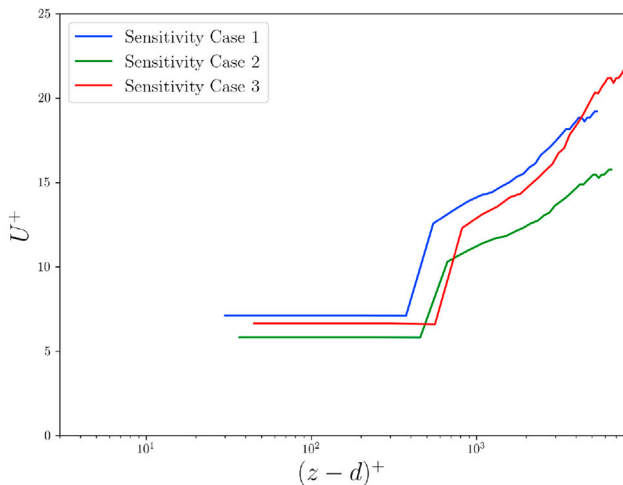
3.2.4. Sensitivity to z_0

From mathematical and theoretical considerations, the height for the centre of the first layer of computational grid adjacent to the wall z_p should be chosen such that $z_0 < z_p/30$ on the grounds that roughness elements with characteristic length $h \sim 10z_0$ should be constrained well within the first layer of the computational grid adjacent to the wall (Blocken et al., 2007; Aboshosha et al., 2015a). To test the VLES model requirement for such a condition, z_0 has been increased gradually to correspond to $z_0 = z_p/30$ (Case 1), $z_0 = z_p/6$ (Case 2), and $z_0 = z_p/3$ (Case 3) while the first layer grid height is kept constant. The VLES model sensitivity to the choice of z_0 is investigated using grid level III and a first grid layer height that corresponded to $(z - d)^+ = 133 - 151$ for $z_0 = 0.0005$ m. Although no experimental data is available to compare the model output with such variation of z_0 , we have plotted the non-dimensionalized horizontal mean velocity vs. non-dimensionalized

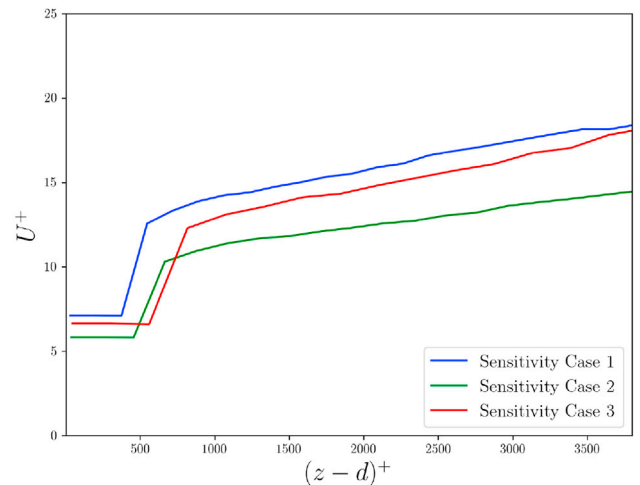
wall-normal distance on profile 4 for various choices of z_0 in Fig. 13. It is found that with increasing z_0 a numerically stable solution can be obtained and that the mean horizontal velocity profile resembles that of the power law. With increasing z_0 , the non-dimensionalized mean horizontal velocity decreases, consistent with the physical explanation that, all other parameters being equal, this reduction is due to increased drag on the flow associated with higher aerodynamic roughness length. Although physically plausible and numerically stable, it is not recommended to use the VLES model with $z_0 > z_p/30$ to constrain the actual roughness element characteristic length h well inside the first layer of grid.

4. Conclusions and future work

A Very Large Eddy Simulation (VLES) model was developed for the



(a) Logarithmic scale



(b) Linear scale

Fig. 13. : Sensitivity of mean horizontal velocity to the choice of z_0 . Results for grid level III on profile 4 are shown for Case 1 ($z_0 = z_p/30$), Case 2 ($z_0 = z_p/6$), and Case 3 ($z_0 = z_p/3$) both in logarithmic (a) and linear (b) scales.

investigation of the Atmospheric Boundary Layer (ABL). The objectives for the model required that the model 1) should be reductionist requiring minimum number of input constants, 2) should simulate the anisotropy of turbulence, 3) should resolve the energy cascade over at least two orders of magnitude of wave numbers, 4) should demonstrate that the correlation for velocity fluctuation components are wave-number dependent, 5) should avoid resolving turbulence near walls, and 6) should exhibit a low adaptation distance. This model included a synthetic vortex method for the inlet boundary condition with the capability to vary the eddy length and time scales as input parameters using two constants only. The model incorporated a one-equation Turbulence Kinetic Energy (TKE) parameterization for the Sub-Grid Scale (SGS) formulation. A rough-wall boundary condition was also included for simulation of airflow over rough surfaces. In summary, the model met all the requirements stated in the objectives.

For wall-resolving simulations, it was found that the profiles of mean velocity and turbulence velocity statistic were in reasonable agreement with the experimental observations. Four grid resolutions were tested with $N = 1,000,000$, $N = 562,500$, $N = 250,000$, and $N = 62,500$ control volumes. The model performance was acceptable on the grid as coarse as $N = 250,000$ control volumes, where more than 80% of the TKE was resolved in the domain interior. In general the adaptation distance for most flow quantities was between two to four boundary layer heights δ , depending on the quantity of interest. This adaptation distance is considered short in comparison to other synthetic eddy method inlet boundary conditions found in the literature.

For wall-resolving simulations, the parameters controlling eddy length and time scales were studied for the synthetic vortex method. It was found that new eddies must be sampled at every model timestep for most accurate results. A sensitivity study revealed the response of the model solutions to the inlet eddy parameters. While mean velocity profiles were not changed significantly, turbulence variances and Reynolds stress were observed to shift slightly in magnitude as the inlet eddy parameters were changed. On the other hand, changing the SGS parameterization resulted in more acute sensitivities in both mean and turbulence profiles of momentum-related quantities.

For rough-wall simulations, the first layer of computational grid adjacent to the wall was coarsened independently, while the grid resolution in the interior of the domain was kept constant at $N = 250,000$ control volumes. Contrary to wall-resolving simulations, where new eddies must be sampled at every model timestep iteration, it was found that the eddy time scale at the inlet synthetic vortex method must be increased to produce accurate results. It was found that the model reproduced wind tunnel profiles of mean velocity and velocity statistics if non-dimensional wall units associated with the first layer of the computational grid was from about 40 to 150. It was found that beyond this range of wall units the wall function and consequently the VLES model could not accurately reproduce the wind tunnel experimental observations. However, these results are not conclusive in setting an upper limit for non-dimensional wall units for the successful or unsuccessful application of wall functions with the VLES model. In this regard, further investigation is required by applying the model to more realistic ABL flows.

It was observed that the model partially matches the spectra associated with the energy-containing and inertial subranges for velocity fluctuation variances and covariances over more than two orders of magnitude of wave numbers. Furthermore, the model seems to show the anisotropy of ABL flows by exhibiting different variances in the stream-wise and wall-normal directions in agreement with other LES studies. The coherency of the flow was not analyzed in detail, but it was observed that the velocity fluctuation correlations are wave-number dependent, with higher correlations for low wave numbers. As a proxy, this is consistent with most coherent flow simulations found in the LES literature.

The VLES model developed can be implemented for various industrial applications where it may be impractical to perform high resolution

simulations or to develop complex precursor or synthetic methods for the inlet boundary condition. However, since coherency was not specifically studied, the model is most suitable for transport problems (e.g. air pollution dispersion) as opposed to wind-induced structural loading, which requires further analysis. Future development of this model can extend the simulation of transport phenomena to heat (e.g. stable ABLs) and passive scalar transport as well. In addition, the model should be tested for full scale ABL simulations.

Funding

This work was supported by the Discovery Grant program from the Natural Sciences and Engineering Research Council (NSERC) of Canada (401231); Canadian Natural (CN) (053451); Government of Ontario through the Ontario Centres of Excellence (OCE) under the Alberta-Ontario Innovation Program (AOIP) (053450); and Emission Reduction Alberta (ERA) (053498). OCE is a member of the Ontario Network of Entrepreneurs (ONE).

Acknowledgements

The authors are indebted to John D. Wilson, Department of Earth and Atmospheric Sciences, University of Alberta, for a careful review of the manuscript prior to submission. In-kind technical support for this work was provided by Rowan Williams Davies & Irwin Inc. (RWDI).

Appendix A. Supplementary data

Supplementary data to this article can be found online at <https://doi.org/10.1016/j.jweia.2018.10.014>.

References

- Aboshosha, H., Bitsuamlak, G., El Damatty, A., 2015a. LES of ABL flow in the built-environment using roughness modeled by fractal surfaces. *Sustain. Cities Soc.* 19, 40–60.
- Aboshosha, H., Elshaer, A., Bitsuamlak, G.T., El Damatty, A., 2015b. Consistent inflow turbulence generator for LES evaluation of wind-induced responses for tall buildings. *J. Wind Eng. Ind. Aerod.* 142, 198–216.
- Aliabadi, A.A., 2018. Theory and Applications of Turbulence: a Fundamental Approach for Scientists and Engineers. Amir A. Aliabadi Publications, Guelph, Ontario, Canada.
- Aliabadi, A.A., Krayenhoff, E.S., Nazarian, N., Chew, L.W., Armstrong, P.R., Afshari, A., Norford, L.K., 2017. Effects of roof-edge roughness on air temperature and pollutant concentration in urban canyons. *Boundary-Layer Meteorol.* 164, 249–279.
- Aliabadi, A.A., Moradi, M., Clement, D., Lubitz, W.D., Gharabaghi, B., 2018. Flow and temperature dynamics in an urban canyon under a comprehensive set of wind directions, wind speeds, and thermal stability conditions. *Environ. Fluid Mech.* <https://doi.org/10.1007/s10652-018-9606-8>.
- Amir, M., Castro, I.P., 2011. Turbulence in rough-wall boundary layers: universality issues. *Exp. Fluids* 51, 313–326.
- Anderson, W., Meneveau, C., 2010. A large-eddy simulation model for boundary-layer flow over surfaces with horizontally resolved but vertically unresolved roughness elements. *Boundary-Layer Meteorol.* 137, 397–415.
- Benhamadouche, S., Jarrin, N., Addad, Y., Laurence, D., 2006. Synthetic turbulent inflow conditions based on a vortex method for large-eddy simulation. *Prog. Comput. Fluid Dynam. Int. J.* 6, 50–57.
- Blocken, B., Stathopoulos, T., Carmeliet, J., 2007. CFD simulation of the atmospheric boundary layer: wall function problems. *Atmos. Environ.* 41, 238–252.
- Blocken, B., Stathopoulos, T., Carmeliet, J., Hensen, J.L., 2011. Application of computational fluid dynamics in building performance simulation for the outdoor environment: an overview. *J. Build. Perf. Simulat.* 4, 157–184.
- Buckingham, S., Koloszar, L., Bartosiewicz, Y., Winkelmann, G., 2017. Optimized temperature perturbation method to generate turbulent inflow conditions for LES/DNS simulations. *Comput. Fluids* 154, 44–59.
- Cao, S., 2014. Advanced physical and numerical modeling of atmospheric boundary layer. *J. Civ. Eng. Res.* 4, 14–19.
- Castro, H.G., Paz, R.R., 2013. A time and space correlated turbulence synthesis method for large eddy simulations. *J. Comput. Phys.* 235, 742–763.
- Castro, H.G., Paz, R.R., Mroginski, J.L., Storti, M.A., 2017. Evaluation of the proper coherence representation in random flow generation based methods. *J. Wind Eng. Ind. Aerod.* 168, 211–227.
- Cheng, H., Castro, I.P., 2002. Near wall flow over urban-like roughness. *Boundary-Layer Meteorol.* 104, 229–259.
- Fernholz, H., Finley, P.J., 1996. The incompressible zero-pressure-gradient turbulent boundary layer: an assessment of the data. *Prog. Aero. Sci.* 32, 245–311.

- Fröhlich, J., Mellen, C.P., Rodi, W., Temmerman, L., Leschziner, M.A., 2005. Highly resolved large-eddy simulation of separated flow in a channel with streamwise periodic constrictions. *J. Fluid Mech.* 526, 19–66.
- Graf, A., van de Boer, A., Moene, A., Vereecken, H., 2014. Intercomparison of methods for the simultaneous estimation of zero-plane displacement and aerodynamic roughness length from single-level eddy-covariance data. *Boundary-Layer Meteorol.* 151, 373–387.
- Greenshields, C.J., 2015. OpenFOAM: the Open Source CFD Toolbox, User Guide, Version 3.0.1. Technical Report. OpenFOAM Foundation Ltd, PO Box 56676, London, W13 3DB, United Kingdom.
- Huang, S.H., Li, Q.S., Wu, J.R., 2010. A general inflow turbulence generator for large eddy simulation. *J. Wind Eng. Ind. Aerod.* 98, 600–617.
- Jarrin, N., 2008. Synthetic Inflow Boundary Conditions for the Numerical Simulation of Turbulence.
- Jiménez, J., 2004. Turbulent flows over rough walls. *Annu. Rev. Fluid Mech.* 36, 173–196.
- Kaimal, J.C., Wyngaard, J.C., Izumi, Y., Coté, O.R., 1972. Spectral characteristics of surface-layer turbulence. *Q. J. Roy. Meteorol. Soc.* 98, 563–589.
- Kaimal, J.C., Wyngaard, J.C., Haugen, D.A., Coté, O.R., Izumi, Y., Caughey, S.J., Readings, C.J., 1976. Turbulence structure in the convective boundary layer. *J. Atmos. Sci.* 33, 2152–2169.
- Kays, W.M., Crawford, M.E., 1993. *Convective Heat and Mass Transfer*, third ed. McGraw-Hill Inc, New York.
- Kent, C.W., Grimmond, S., Barlow, J., Gatey, D., Kotthaus, S., Lindberg, F., Halios, C.H., 2017. Evaluation of urban local-scale aerodynamic parameters: implications for the vertical profile of wind speed and for source areas. *Boundary-Layer Meteorol.* 164, 183–213.
- Kim, Y., Castro, I.P., Xie, Z.-T., 2013. Divergence-free turbulence inflow conditions for large-eddy simulations with incompressible flow solvers. *Comput. Fluids* 84, 56–68.
- Krayenhoff, E.S., Santiago, J.-L., Martilli, A., Christen, A., Oke, T.R., 2015. Parametrization of drag and turbulence for urban neighbourhoods with trees. *Boundary-Layer Meteorol.* 156, 157–189.
- Krogstad, P.A., Efron, V., 2012. About turbulence statistics in the outer part of a boundary layer developing over two-dimensional surface roughness. *Phys. Fluids* 24, 075112.
- Launder, B.E., Spalding, D.B., 1974. The numerical computation of turbulent flows. *Comput. Methods Appl. Mech. Eng.* 3, 269–289.
- Li, X.-X., Liu, C.-H., Leung, D.Y.C., 2008. Large-eddy simulation of flow and pollutant dispersion in high-aspect-ratio urban street canyons with wall model. *Boundary-Layer Meteorol.* 129, 249–268.
- Li, X.-X., Britter, R.E., Koh, T.Y., Norford, L.K., Liu, C.-H., Entekhabi, D., Leung, D.Y.C., 2010. Large-eddy simulation of flow and pollutant transport in urban street canyons with ground heating. *Boundary-Layer Meteorol.* 137, 187–204.
- Li, X.-X., Britter, R.E., Norford, L.K., Koh, T.-Y., Entekhabi, D., 2012. Flow and pollutant transport in urban street canyons of different aspect ratios with ground heating: large-eddy simulation. *Boundary-Layer Meteorol.* 142, 289–304.
- Li, X.-X., Britter, R.E., Norford, L.K., 2015. Transport processes in and above two-dimensional urban street canyons under different stratification conditions: results from numerical simulation. *Environ. Fluid Mech.* 15, 399–417.
- Lund, T.S., Wu, X., Squires, K.D., 1998. Generation of turbulent inflow data for spatially-developing boundary layer simulations. *J. Comput. Phys.* 140, 233–258.
- Martilli, A., Clappier, A., Rotach, M.W., 2002. An urban surface exchange parameterisation for mesoscale models. *Boundary-Layer Meteorol.* 104, 261–304.
- Mathey, F., Cokljat, D., Bertoglio, J.P., Sergent, E., 2006. Assessment of the vortex method for large eddy simulation inlet conditions. *Prog. Comput. Fluid Dynam. Int. J.* 6, 58–67.
- Mayor, S.D., Spalart, P.R., Tripoli, G.J., 2002. Application of a perturbation recycling method in the large-eddy simulation of a mesoscale convective internal boundary layer. *J. Atmos. Sci.* 59, 2385–2395.
- Mellor, G.L., Yamada, T., 1974. A hierarchy of turbulence closure models for planetary boundary layers. *J. Atmos. Sci.* 31, 1791–1806.
- Mirocha, J., Kosović, B., Kiril, G., 2014. Resolved turbulence characteristics in large-eddy simulations nested within mesoscale simulations using the Weather Research and Forecasting model. *Mon. Weather Rev.* 142, 806–831.
- Nozawa, K., Tamura, T., 2002. Large eddy simulation of the flow around a low-rise building immersed in a rough-wall turbulent boundary layer. *J. Wind Eng. Ind. Aerod.* 90, 1151–1162.
- Poletto, R., Craft, T., Revell, A., 2013. A new divergence free synthetic eddy method for the reproduction of inlet flow conditions for LES. *Flow, Turbul. Combust.* 91, 519–539.
- Pope, S.B., 2000. *Turbulent Flows*. Cambridge University Press, Cambridge, U.K.
- Raupach, M.R., 1992. Drag and drag partition on rough surfaces. *Boundary-Layer Meteorol.* 60, 375–395.
- Raupach, M.R., Antonia, R.A., Rajagopalan, S., 1991. Rough-wall turbulent boundary layers. *Appl. Mech. Rev.* 44, 1–25.
- Ricci, M., Patruno, L., de Miranda, S., 2017. Wind loads and structural response: benchmarking LES on a low-rise building. *Eng. Struct.* 144, 26–42.
- Roache, P.J., 1997. Quantification of uncertainty in computational fluid dynamics. *Annu. Rev. Fluid Mech.* 29, 123–160.
- Sergent, M.E., 2002. Vers une méthodologie de couplage entre la simulation des grandes échelles et les modèles statistique.
- Smagorinsky, J., 1963. General circulation experiments with the primitive equations: I. The basic equations. *Mon. Weather Rev.* 91, 99–164.
- Spalart, P.R., 1988. Direct simulation of a turbulent boundary layer up to $Re_\theta=1410$. *J. Fluid Mech.* 187, 61–98.
- Stull, R.B., 1988. *An Introduction to Boundary Layer Meteorology*. Kluwer Academic Publishers, Dordrecht, The Netherlands.
- Tabor, G.R., Baba-Ahmadi, M.H., 2010. Inlet conditions for large eddy simulation: a review. *Comput. Fluids* 39, 553–567.
- Taylor, G.I., 1938. The spectrum of turbulence. *Proc. Roy. Soc. Lond. A* 164, 476–490.
- Thomas, T.G., Williams, J.J.R., 1999. Generating a wind environment for large eddy simulation of bluff body flows. *J. Wind Eng. Ind. Aerod.* 82, 189–208.
- van Driest, E.R., 1956. On turbulent flow near a wall. *J. Aeronaut. Sci.* 23, 1007–1011.
- von Kármán, T., 1948. Progress in the statistical theory of turbulence. *Proc. Natl. Acad. Sci. U. S. A* 34, 530–539.
- Xie, B., 2016. Improved Vortex Method for LES Inflow Generation and Applications to Channel and Flat-plate Flows.